

**Spatio-temporal variations in global surface soil moisture based on multiple datasets:**

**Intercomparison and climate drivers**

Yansong Guan<sup>1</sup>, Xihui Gu<sup>1,2,3,4,5,6,7\*</sup>, Louise J. Slater<sup>8</sup>, Jianfeng Li<sup>9\*</sup>, Dongdong Kong<sup>1,7</sup>, Xiang

Zhang<sup>10</sup>

1. School of Computer Science & School of Environmental Studies, China University of Geosciences, Wuhan 430074, China;

2. Key Laboratory of Meteorological Disaster Ministry of Education & Collaborative Innovation Center on Forecast and Evaluation of Meteorological Disasters, Nanjing University of Information Science & Technology, Nanjing 210044, China;

3. Institute of Arid Meteorology, China Meteorological Administration, Louzhou, China, 730020;

4. The National Key Laboratory of Water Disaster Prevention, Nanjing Hydraulic Research Institute, Nanjing 210029, China;

5. SongShan Laboratory, Zhengzhou 450046, China;

6. State Key Laboratory of Loess and Quaternary Geology, Institute of Earth Environment, CAS, Xi'an 710061, China;

7. Centre for Severe Weather and Climate and Hydro-geological Hazards, Wuhan 430074, China;

8. School of Geography and the Environment, University of Oxford, Oxford, UK;

9. Department of Geography, Hong Kong Baptist University, Hong Kong, China;

10. National Engineering Research Center of Geographic Information System, School of Geography and Information Engineering, China University of Geosciences, Wuhan 430074, China.

**\*Corresponding authors:**

Xihui Gu, Email: guxh@cug.edu.cn

Jianfeng Li, Email: jianfengli@hkbu.edu.hk

**Highlights:**

- The first study to comprehensively analyze and compare the long-term variations of global surface soil moisture among multiple datasets;
- Pervasive surface soil moisture drying is found across the globe, especially in humid-arid transitional regions, in most datasets;
- Warming plays a primary role in global surface soil moisture drying in most datasets, especially GLEAM.

**Abstract:** Accurate soil moisture datasets are essential to understand the impacts of climate change. However, few studies have evaluated the consistency and drivers of long-term trends in soil moisture among different dataset types (satellite, assimilation, reanalysis, and climate model) at the global scale. Here we analyze the spatio-temporal variations of global surface soil moisture and associated climate dynamics over 1980-2020 using multiple soil moisture datasets, i.e., multi-satellite assimilated remote sensing datasets (ESA CCI), simulated soil moisture based on LSMs (GLDAS, GLEAM, CMIP6), and reanalysis (ECMWF ERA5, MERRA2, CRA-Land). Most of these datasets indicate pervasive drying of global surface soil moisture over the last four decades. Prominent soil moisture drying is detected in North America, Europe, northeastern Asia, North Africa, and the Arabian Peninsula. The cross-correlations among the five synthetic soil moisture datasets are the

highest between GLEAM and the reanalysis datasets. Using the Aridity Index (AI, the ratio between annual total precipitation and potential evapotranspiration), we find that soil moisture drying is the most intensive in the humid-arid transitional regions with AI ranging 0.8-1.2. Surface soil moisture drying is primarily driven by increases in temperature, followed by ENSO, as indicated by Maximum Covariance Analysis (MCA). However, the significance of the impact of ENSO on soil moisture variability is sensitive to the choice of soil moisture dataset used in the MCA.

**Key words:** Soil moisture; Climate change; Dynamical processes; Maximum Covariance Analysis; ENSO

## 1. Introduction

Soil moisture is a key state variable for hydrological processes in terms of its influence on land-atmosphere water and energy exchanges. Within the hydrological cycle, soil moisture availability acts as a major constraint on evapotranspiration from the land surface (Seneviratne et al., 2010; Z. Liu et al., 2021; J. Liu et al., 2021). Over longer periods, soil moisture also preconditions the likelihood of hydrological extremes such as flooding and drought (Slater and Villarini, 2016; Teuling, 2018; Brunner et al., 2021; McKinnon et al., 2021; Feng et al., 2022; Guan et al., 2022; Kong et al., 2022; Yin et al., 2022 and 2023; Min et al., 2023). Thus, accurate monitoring and evaluation of soil moisture changes is essential to improve the accuracy of simulations and forecasts of both climatic and hydrological processes.

Soil moisture datasets can be based on or developed using different techniques, including *in-situ* measurements, satellite remote sensing, and model simulations (e.g., Qin et al., 2009; Cheng et

al., 2015; Chen et al., 2016; Meng et al., 2021). Due to the lack of a high-density network of long-term soil moisture observations at the global scale, *in-situ* measurements are usually not employed in global soil moisture analyses. Instead, global studies typically employ the recently released multi-satellite assimilated remote sensing datasets (i.e., European Space Agency Climate Change Initiative (ESA CCI)) to assess long-term changes in soil moisture globally (Liu et al., 2011; Dorigo et al., 2012; Feng, 2016; Meng et al., 2021), because these satellite observations have a record length of multiple decades. One of the drawbacks of satellite observations is that only surface soil moisture can be acquired (Entekhabi et al., 2010; Kerr et al., 2010). A number of simulated soil moisture datasets have been developed based on the outputs of land surface models (LSMs) in offline or online modes, such as the Global Land Data Assimilation System (GLDAS; Rodell et al., 2004), the Global Land Evaporation Amsterdam Model (GLEAM; Martens et al., 2017), and the Coupled Model Intercomparison Project Phase 5/6 (CMIP5; Taylor et al., 2012; CMIP6; Eyring et al., 2016). Reanalysis datasets are another important source of soil moisture information, and include the European Centre for Medium-Range Weather Forecasts' fifth generation atmospheric reanalysis of the global climate (ERA5; Hoffmann et al., 2019), the Modern Era Retrospective-analysis for Research and Applications version 2 (MERRA2; Rienecker et al., 2011), and China Meteorological Administration global Land surface Reanalysis dataset (CRA-Land).

Investigations on how soil moisture changes in space and time are beneficial for understanding the evolution of drought, associated climatic drivers, and soil moisture-atmosphere interactions (Orth et al., 2016, 2017; Rasmijn et al., 2018; Humphrey et al., 2021; M. Li et al., 2021; Jiang et al., 2022). The positive feedback between temperature and soil moisture is strong: high temperature tends to accelerate soil moisture drying, which further increases temperature (Teuling, 2018). This

89 feedback stresses the importance of the state of (and changes in) soil moisture for land-atmosphere  
90 interaction. For example, the intensity and frequency of heatwave events are enhanced by low soil  
91 moisture; in Russia, low soil moisture was found to elevate the risk of the 2010 extreme heatwave  
92 event occurrences sixfold (Hauser et al., 2016). Soil moisture-atmosphere interactions can also alter  
93 the initiation of convective precipitation by affecting the partitioning of sensible and latent heat  
94 (Ford et al., 2015). These results highlight the importance of accurately assessing variations in soil  
95 moisture under global warming to understand climate change impacts on the hydrological cycle.

96 Traditionally, spatio-temporal changes in surface soil moisture and their relationships with  
97 climatic drivers such as precipitation and temperature have been analyzed by using satellite  
98 observations and model simulations globally and regionally (Dorigo et al., 2012; Cheng and Huang  
99 2016; Zhang et al., 2018; Gu et al., 2019a). However, investigations of large-scale and long-term  
100 surface soil moisture variations have been generally based on individual datasets without  
101 considering spatio-temporal variations in soil moisture among different datasets and the drivers of  
102 such variability. Although the highly heterogeneous nature of soil moisture has received extensive  
103 attention, previous studies have mainly focused on the biases by comparing the datasets against *in-*  
104 *situ* measurements using error/bias indices, such as mean absolute error, mean bias error, and root-  
105 mean-square error (Albergel et al., 2012; Dorigo et al., 2015; Karthikeyan et al., 2017a; Gu et al.,  
106 2019b).

107 Few studies have evaluated the consistency or discrepancy of long-term trends in soil moisture  
108 among different datasets (Orlowsky and Seneviratne, 2013; K. Rötzer et al., 2015; Deng et al., 2020;  
109 M. Li et al., 2020). For example, M. Li et al. (2020) compared the long-term trends in soil moisture  
110 layers from 5 cm to 100 cm during 1979-2017 between five reanalysis datasets and *in-situ*

observations, and found that the reanalyses showed statistically significant correlations with observations at the in-situ scale. Deng et al. (2020) compared the long-term daily surface soil moisture during 1979-2017 among ESA CCI, GLDAS, and one reanalysis dataset, and found consistent drying trends especially during 2001-2017. However, the previous evaluations of long-term changes of soil moisture have the following limitations: (a) a focus on network or regional scales (Escorihuela et al., 2016; Holgate et al., 2016; Das et al., 2019; Li et al., 2021; Yang et al., 2021); (b) an incomplete selection of soil moisture datasets, lacking GLEAM and the newly released reanalysis datasets (e.g., CRA-Land and ERA5; Rötzer et al., 2015; Liu et al., 2019); and (c) a lack of comparison with the recently released CMIP6 data (Li et al., 2020; Jiang et al., 2022). Hence, the heterogeneity of long-term variations in soil moisture among the most comprehensive existing global datasets (i.e., ESA CCI, GLEAM, reanalysis, GLDAS, and CMIP6) and the impacts of this heterogeneity on the relations between soil moisture and climatic factors (such as precipitation and temperature) remain unknown.

The primary goals of this study are thus (1) to analyze and compare temporal variations of surface soil moisture from different datasets; (2) to analyze the relationships between surface soil moisture and climatic drivers; and (3) to explore the climate dynamics underpinning soil moisture variations. This work aims to reveal which long-term variations in surface soil moisture are consistent across different types of datasets (satellite, model simulations and reanalysis), to increase confidence in the assessment of soil moisture changes from these datasets, given the lack of global-scale *in-situ* measurements. Furthermore, the study also reveals consistent/inconsistent relationships between climatic drivers and long-term variations in soil moisture, providing insights for dataset developers to further enhance the quality of soil moisture datasets. The new generation of climate

models improving the simulation of soil moisture would strengthen the understanding and prediction of extreme events (e.g., heatwaves) (Miralles et al., 2014).

## **2. Data**

A number of hydroclimatic variables are considered in this study, including soil moisture, monthly weather data (i.e., precipitation (PRCP), surface air temperature (SAT), and potential evapotranspiration (PET)), and large-scale environmental variables (i.e., geopotential height, wind, and sea surface temperature (SST)). The soil moisture and weather data are aggregated to annual means and interpolated to a uniform spatial resolution. The data of these variables during the period of 1980-2020 are extracted to conduct our analyses.

### **2.1 Soil moisture datasets**

Soil moisture datasets were collected from satellite-based sources (ESA CCI combined soil moisture dataset, version 06.1), reanalysis (i.e., ERA5, MERRA2, and CRA-Land) (Table 1), and simulations (three simulated products of GLDAS version 2.0/2.1 and eighteen CMIP6 GCMs; Tables 1-2). Among these soil moisture datasets, only the ESA CCI dataset was scaled (using the soil moisture range of the GLDAS-Noah dataset). Despite scaling, the ESA CCI product can be still used as an independent dataset for computing correlation statistics and long-term variations (see more details at <https://www.esa-soilmoisture-cci.org/index.php?q=node/136>). The daily ESA CCI soil moisture from the combined product was averaged into annual means. More details about the ESA CCI data are available at <http://www.esa-soilmoisture-cci.org>. The GLEAM soil moisture product is produced by the Global Land Evaporation Amsterdam Model (i.e., version 3.7), a

collection of algorithms that take into account the influence of soil moisture on the process of evaporation. GLDAS is a widely used soil moisture dataset, where the soil moisture information is simulated by LSMs driven by satellite- and ground-based observations (Rui and Beaudoin, 2016). We obtained monthly soil moisture of the top layer output from three LSMs (i.e., 2 cm for Community Land Model (CLM), 30 cm for Infiltration Capacity (VIC) and 10cm for Noah (NOAH)) in GLDAS version 2.0 and 2.1 from <https://disc.sci.gsfc.nasa.gov/datasets?keywords=GLDAS>. The three reanalysis datasets, i.e., ERA5, MERRA2, and CRA-Land, were recently released by the European Centre for Medium Range Weather Forecasts (Hoffmann et al., 2019), NASA (National Aeronautics and Space Application), and the China Meteorological Data Service Centre, respectively. Monthly soil moisture in the top layer (i.e., 7 cm for ERA5, 2 cm for MERRA2, and 10 cm for CRA-Land) was extracted from the three reanalysis datasets for this study.

We collected monthly soil moisture from eighteen GCMs under the historical and the Shared Socio-economic Pathway 2-4.5 scenarios (Table 2). Only the top layer soil moisture obtained from the first ensemble run (i.e., “r1i1p1f1”) of each GCM was used. The SSP2-4.5 simulations for the period 2015-2020 were used to extend the historical simulations (the time series of which ends in 2014). This method to extend the historical scenario of GCM outputs has been adopted in previous studies (IPCC, AR5; Sun et al., 2016; Yuang and Quiring 2017). It should be noted that terrestrial and atmospheric components are fully coupled in these GCMs. A summary of attributes of these datasets is shown in Tables 1 and 2.

Furthermore, we collected ground-based measurements with a top layer depth of 0-10 cm in kg/kg from 778 Agricultural Meteorological Stations across China. These agricultural meteorological stations are mostly located in agricultural areas and provide monthly soil moisture



values during the period 1992-2010. Because the in-situ observations are scarce during the cold season, we focus on the soil moisture means in March-October for the five global datasets in our study. More details about this ground-based dataset are available at <http://www.cma.gov.cn/2011qxfw/2011qsjgx/>. The ground-based measurements are employed to assess the performance of soil moisture in ESA CCI, GLDAS, reanalysis, and CMIP6 (see Text S1, Figs. S1 and S2 in Supplementary materials).

## **2.2 Monthly weather data**

Monthly weather data including PRCP, SAT, and PET with  $0.5^{\circ} \times 0.5^{\circ}$  resolution were obtained from the Climatic Research Unit (CRU) Time-Series (TS) dataset, version CRU TS4.06 (Table 3). The dataset is available at <https://catalogue.ceda.ac.uk/uuid/e0b4e1e56c1c4460b796073a31366980>. PRCP and SAT data are produced using station-based measurements, and PET data is estimated based on the gridded variables (e.g., PRCP and SAT data) through the Penman–Monteith formula (Harris et al., 2020). The CRU PRCP and PET datasets are also employed to calculate Aridity Index (AI) which is defined as annual total PRCP/annual total PET (Cheng et al., 2016). Moreover, PRCP and SAT outputs from CMIP6 GCMs are also used in the CMIP6-related analyses, and PET is also estimated by the Penman–Monteith formula using the CMIP outputs, i.e., maximum near-surface air temperature (tasmax), daily minimum near-surface air temperature (tasmin), near-surface relative humidity (hurs), near-surface wind speed (sfcWind), surface upward sensible heat flux (hfss), and surface upward latent heat Flux(hfls).

## **2.3 Large-scale environmental variables data**

Monthly values of geopotential height and wind were obtained from the ERA5 reanalysis data.

The spatial resolution of the ERA5 reanalysis data is  $0.25^{\circ} \times 0.25^{\circ}$  (Table 3). We collected global monthly sea surface temperature analysis data from the Japan Meteorological Agency (i.e., COBE SST with  $1^{\circ} \times 1^{\circ}$  spatial resolution; Table 3). These same large-scale environmental variables were also obtained from CMIP6 GCMs for the CMIP6-related analyses.

### **3. Methods**

#### **3.1 Data pre-processing**

We pre-processed these soil moisture datasets by homogenizing them in terms of spatial resolution, record length, layer depths and units. To reduce the influence of discrepancies in layer depth on the inter-comparison, only soil moisture in the top layer was extracted for all datasets, following Bi et al. (2016). The depths of the top layer range between 0.02- 0.3 m (see Tables 1 and 2). The units used for the inter-comparison are  $\text{kg/m}^2$  and  $\text{m}^3/\text{m}^3$  (see Tables 1 and 2). The soil moisture values in units of  $\text{kg/m}^2$  were transformed to the volumetric unit ( $\text{m}^3/\text{m}^3$ ) as  $S/rH$ , where  $S$  represents soil moisture (units:  $\text{kg/m}^2$ ),  $r$  represents the depth of soil layer depth (units: m), and  $H$  represents water density (units:  $\text{kg/m}^3$ ). A bilinear interpolation method was employed to regrid all the gridded soil moisture datasets to a spatial resolution of  $1^{\circ} \times 1^{\circ}$ . The surface soil moisture performance of the ESA CCI, GLEAM, GLDAS, reanalysis, and CMIP6 datasets was assessed relative to the ground-based measurements in China in terms of their long-term means and variations (see Text S1, Figs. S1 and S2 in Supplementary materials).

The ESA CCI data have gaps due to observational frequency inherent in a satellite product. All the grid cells with record length longer than one year have more than 8% of missing data (i.e., observation gaps in the data) (Fig. S3). Less than 40% of global land grid cells have a record length

covering the full selected period (i.e., 1980-2020, 41 years). The percentage of grid cells with more than 30 years of data decreases quickly. Only grid cells with a record length longer than 30 years are considered in this study; most are located between 60° N and 60° S (Fig. S4). To further reduce the impacts of frozen and snow-covered states (Dorigo et al., 2015), the ESA CCI values are masked on days with a daily mean temperature (obtained from the Climate Prediction Center at <https://www.esrl.noaa.gov/psd/data/gridded/data.cpc.globaltemp.html>) of less than zero degrees Celsius (Dorigo et al., 2015).

### **3.2 Spearman correlation coefficient and Sen's slope trend test**

The Spearman correlation coefficient is estimated to quantify temporal correlations among multiple soil moisture datasets. The Sen's slope method is employed to compute linear trends of soil moisture, climate variables (such as PRCP, SAR, PET), and environmental variables (such as geopotential height and wind) during the period of 1980-2020, because it has been successfully applied to detect trends in multiple hydro-climatological variables (Zhang et al., 2014; Gu et al., 2017a, b, c). We use the Spearman test and Mann-Kendall test (Kendall, 1975; Mann, 1945) to estimate the significance level (i.e., p-value) of correlation and trend, respectively. If the p-value is less than 0.05, the correlation/trend is considered as statistically significant.

### **3.3 Maximum Covariance Analysis (MCA)**

Maximum Covariance Analysis (MCA) based on the singular value decomposition (SVD) method has been widely used to extract the coupled modes of two climate variables (Mo, 2003), i.e., the patterns that exhibit the strongest covariability between the two variables being analyzed. A

covariance matrix is constructed by the MCA based on the time series of the two variables, and then a SVD calculation is conducted on the covariance matrix. Finally, similar to the empirical orthogonal decomposition method, the temporal and spatial patterns between the two variables are split in the form of couples. For each couple, there is one temporal mode and a corresponding spatial mode for the first variable, and one temporal mode and one corresponding spatial mode for the other variable. The explained variances are provided for each couple, and help identify which couple is the leading mode. Coherent temporal and spatial patterns of the leading modes are used to detect signals of change in the associated variables (Leonardi et al., 2002). In this study, annual mean SST anomalies in the latitude range of 40°S-60°N and annual mean soil moisture anomalies from each dataset are the input data, and then a covariance matrix is constructed between the SST anomalies and the annual soil moisture anomalies. The SVD is conducted on the covariance matrix, and finally both the SST anomalies and the annual soil moisture anomalies are split to a set of modes including temporal and spatial information.

## **4. Results**

### **4.1 Inter-comparison of surface soil moisture from multiple datasets**

Fig. 1 shows the temporal cross correlations among multiple soil moisture datasets, based on the interannual variations of the soil moisture data. The annual mean soil moisture values are linearly detrended before calculating the temporal correlations. For each dataset pair, we calculate the temporal correlations using all the selected grid cells, and then the median of these temporal correlations is taken as the value of the cross-correlation. It is observed that GLDAS, GLEAM, and reanalysis soil moisture have the highest positive cross-correlations among all datasets, likely

because satellite observations and *in-situ* measurements were merged into GLDAS (Fig. 1). The median values of the temporal cross correlations between ESA CCI and other datasets are almost all in the range of 0.28-0.44, due to the homogeneity of multi-source satellites (Su et al., 2016), missing data, and the uncertainty of retrievals (Liu et al., 2012). Although the ESA CCI soil moisture values were scaled based on the GLDAS-Noah product, ESA CCI still preserves surface soil moisture variations derived from satellite observations (Dorigo et al., 2015). In contrast, due to the inadequate consideration of land surface processes in the model simulations (Wang et al., 2022), the CMIP6 GCMs have low cross-correlation with other datasets.

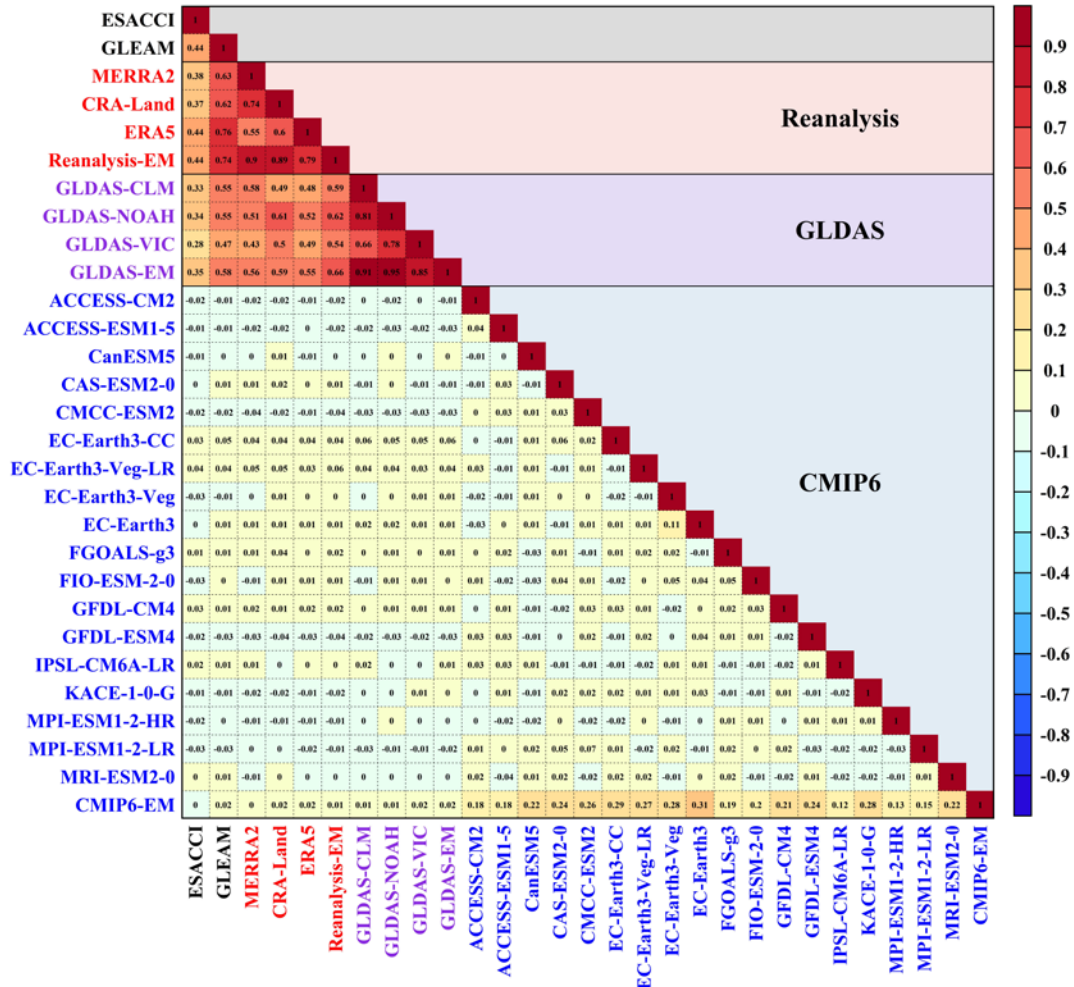


Fig. 1 Cross-correlation between ESA CCI, GLEAM, GLDAS (i.e., CLM, NOAH, and VIC), reanalysis (i.e., ERA5, MERRA2, and CRA-Land), and CMIP6 datasets. GLDAS-EM/Reanalysis-EM/CMIP6-EM indicates the ensemble means of the GLDAS/reanalysis/CMIP6 products.

Fig. 2 shows spatial distributions of Spearman correlation coefficient of annual soil moisture among ESA CCI, GLEAM, GLDAS-EM, and Reanalysis-EM datasets. Most of the grid cells exhibit significant correlations between GLEAM and Reanalysis-EM (ensemble means of three reanalysis datasets), GLEAM and GLDAS-EM (ensemble means of three GLDAS datasets), as well as Reanalysis-EM and GLDAS-EM, in line with the result reflected in Fig. 1. Almost all considered grids show positive correlations between ESA CCI and GLEAM, and ESA CCI and GLDAS-EM, as well as ESA CCI and Reanalysis-EM. The correlations are significant in northeastern Asia and Australia, southern South America, and North America (Fig. 2). Previous studies also indicated high correlations among ESA CCI, GLDAS, and reanalysis in these regions (Albergel et al., 2012; Holgate et al., 2016). We calculate the average correlations of annual soil moisture between one dataset and the others (Fig. S5). The average correlations between Reanalysis-EM and the other datasets perform the best with 82.78% of grids reaching the 0.05 significance level. The percentage of grid cells with significant temporal correlations between GLEAM and the others is very close to that of Reanalysis-EM, while lower temporal correlations can be observed between ESA CCI and the other datasets (63.49% of grids reaching the 0.05 significance level). Spatially, Australia, southern Africa, southern South America, and North America are the areas where all the datasets show a consensus in temporal correlations, while discrepancies can be observed in northern Africa, eastern Asia, central Asia, and Europe.

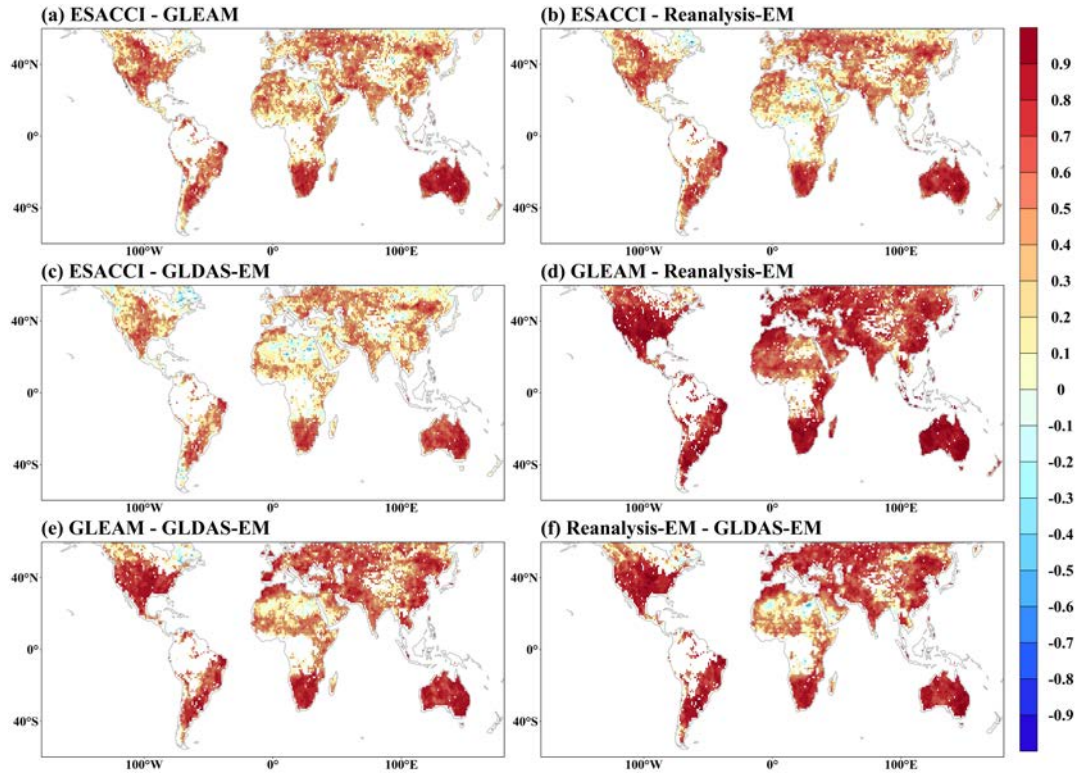


Fig. 2 Spatial distributions of Spearman correlation coefficient of annual soil moisture among ESA CCI, GLEAM, GLDAS-EM, and Reanalysis-EM datasets. Black points indicate areas where the Spearman correlation coefficient is significant at the 0.05 level.

Fig. 3 shows the evolution of spatial correlations of soil moisture. Overall, the spatial correlations between ESA CCI and the other datasets show noticeable increases in the last 10 years, because of the improving quality of the ESA CCI product due to more advanced satellite technologies and retrieval algorithms (Karthikeyan et al., 2017b; Gruber et al., 2019). The spatial correlations between GLDAS and the other datasets are stable in time. There are low inter-annual variations in the spatial correlations between the GLEAM, Reanalysis-EM and CMIP6-EM datasets, reflecting a weaker influence of natural variability on these datasets. The temporal changes in spatial correlations among different soil moisture datasets can reveal critical uncertainties in the underlying data, contributing to discrepancy in long-term trend estimates among different soil moisture datasets.

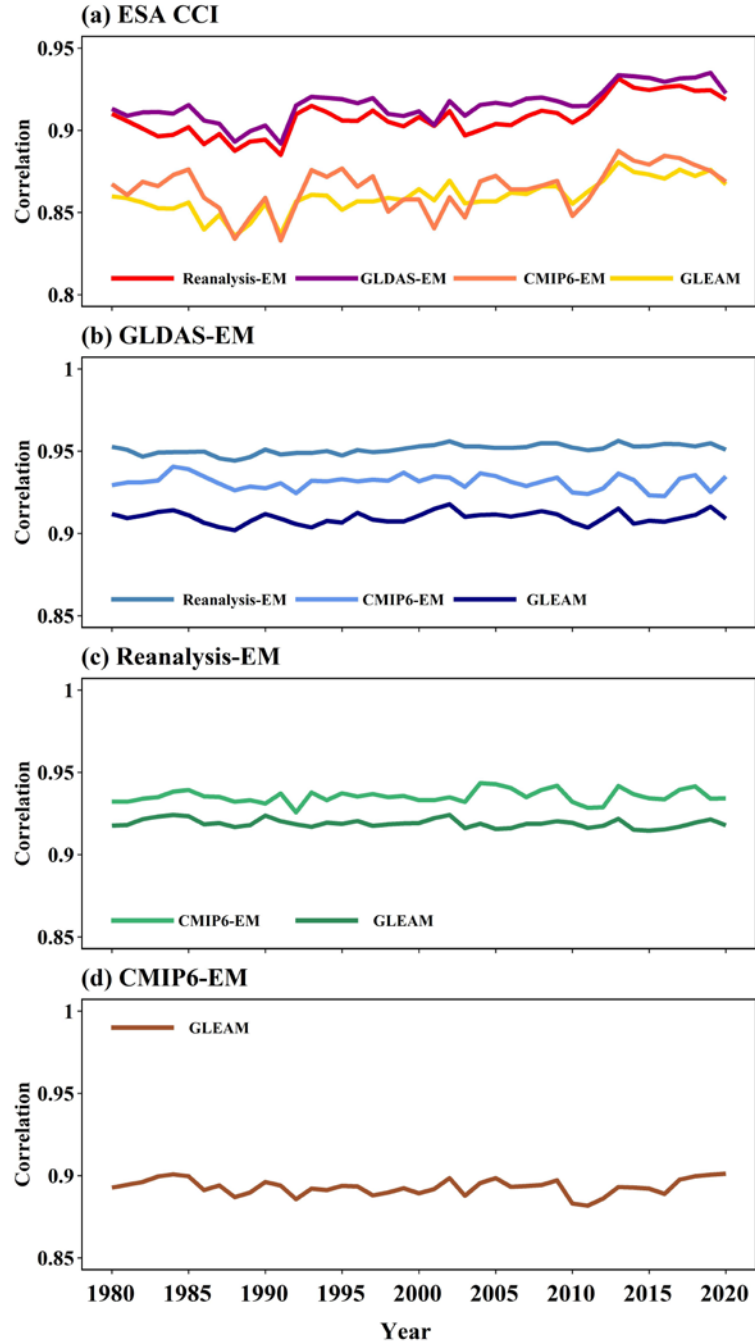


Fig. 3 Temporal changes in spatial correlations between the ESA CCI, GLEAM, GLDAS-EM, Reanalysis-EM, and CMIP6-EM annual soil moisture datasets.

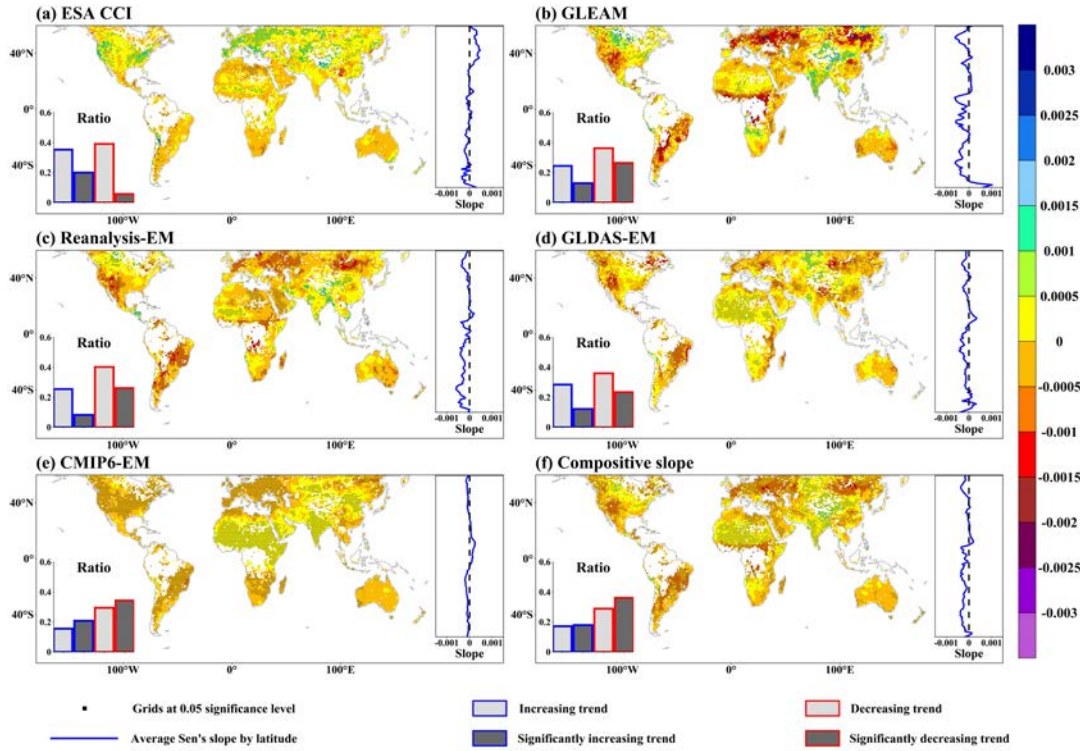
#### 4.2 Spatio-temporal variations in surface soil moisture and their associations with climatic factors

Here, we detect and compare the trends in annual mean soil moisture over 1980-2020 based on multiple datasets (Fig. 4). Most of the datasets agree with widespread surface soil moisture drying



at the global scale, except for ESA CCI in which more than half of the grids (55.21%) show wetting. Compared with the other datasets, the GLEAM and Reanalysis-EM soil moisture indicates more widespread and severe soil moisture drying across the globe, and the magnitudes of soil moisture drying are the largest with strongly negative estimates of Sen's slope averaged by latitude (Fig. 4c). Regional disagreement in variations of soil moisture between GLDAS-EM and GLEAM can be seen in East Asia and Australia (Fig. 4b and d). CMIP6-EM (ensemble means of GCMs) captures the spatial patterns of soil moisture variations with a sign of change that is consistent in most areas with the other datasets, while the magnitude of the variation is noticeably the smallest among all datasets (Fig. 4e). Spatial cross-correlation of the trends in annual soil moisture (computed from Sen's slope) between ESA CCI, GLEAM, Reanalysis-EM, GLDAS-EM, and CMIP6-EM is shown in Fig. S6. Although low spatial correlations are observed between ESA CCI and the other datasets, and between CMIP6-EM and the others, the spatial correlations among GLEAM, Reanalysis-EM, GLDAS-EM are positive and high with a significance level less than 0.01. Despite the inconsistency of regional soil moisture variations among these datasets, the prominent drying in regions such as North America, Europe, northeastern Asia, North Africa and Arabian Peninsula is consistent across the majority of the datasets as shown in Fig. 4f (where the Sen's slope value shown in each grid cell is the average of  $\geq 3$  of the five datasets with the same sign; hereafter referred to as the composite soil moisture). We also count the fraction of all grid cells with the same trend directions, for each dataset pair (Table 4). The highest ratio is found between GLEAM and the other datasets, i.e., in GLEAM, there are on average 60% of grids having consistent trends with the others. ESA CCI is the dataset which has the lowest average ratio (i.e., 0.50) of grid cells with the same sign as other datasets, indicating that soil moisture trends diverge in more than 50% of areas, relative to the other

340 datasets.



341 Fig. 4 Spatial distributions of trends during 1980-2020 in annual soil moisture of ESA CCI, GLEAM,  
 342 GLDAS-EM, Reanalysis-EM, and CMIP6-EM (unit:  $\text{m}^3/\text{m}^3/\text{a}$ ), estimated using Sen's slope. The  
 343 composite slope in (f) is the average of slopes for the grid cells where  $\geq 3$  of the datasets have the  
 344 same sign. The barplot in each subpanel indicates the percentage of grid cells with each sign (i.e.,  
 345 insignificant increase, significant increase, insignificant decrease, and significant decrease) to total  
 346 grids considered. The vertical blue line in each subpanel indicates the Sen's slope averaged by  
 347 latitude. The significance level for the Sen's slope is set as 0.05.

349

350 Since differences in soil moisture variations are detected among different datasets, we further

351 analyze the changes in climatic variables including AI, PRCP, PET and SAT to understand how and

352 why soil moisture changes (Fig. 5). The changes in PRCP and PET in the CRU dataset are verified

353 using observed PRCP from Global Precipitation Climatology Centre (GPCC) and the PET from

354 Abatzoglou et al. (2018) (see Texts S2 and S3, and Fig. S7 in Supplementary materials). Both

355 reanalysis assimilations and model simulations show increasing PET in most areas (Fig. 5e-h), due

356 to the widespread warming across the globe. Because changes in PRCP show substantial spatial

357 differences among datasets (Fig. 5a-b), the changes in AI (computed as  $\text{PRCP}/\text{PET}$ ) can better

reflect variations of climate drying or wetting (Huang et al., 2016). We find similar spatial patterns in the trends in AI and composite soil moisture (Fig. 4f and Fig. 5a-b), suggesting that the ensemble of multiple soil moisture datasets is a more reasonable representation than the individual datasets. The prominent drying soil moisture in western North America, Europe, northeastern Asia, and western and eastern Australia is supported by decreasing AI, where decreasing PRCP can be also observed (Fig. 5c-d and Fig. S8). Increasing precipitation amounts over 1980-2015 in the Sahel were also observed by Biasutti (2019), and this increase can be explained as the response to anomalies in atmospheric circulation and/or increased greenhouse gases (Biasutti 2019). Increases in precipitation are a strong driver of soil moisture wetting. The significant wetting in AI and PRCP in the Sahel region seem to support the results of CMIP6.

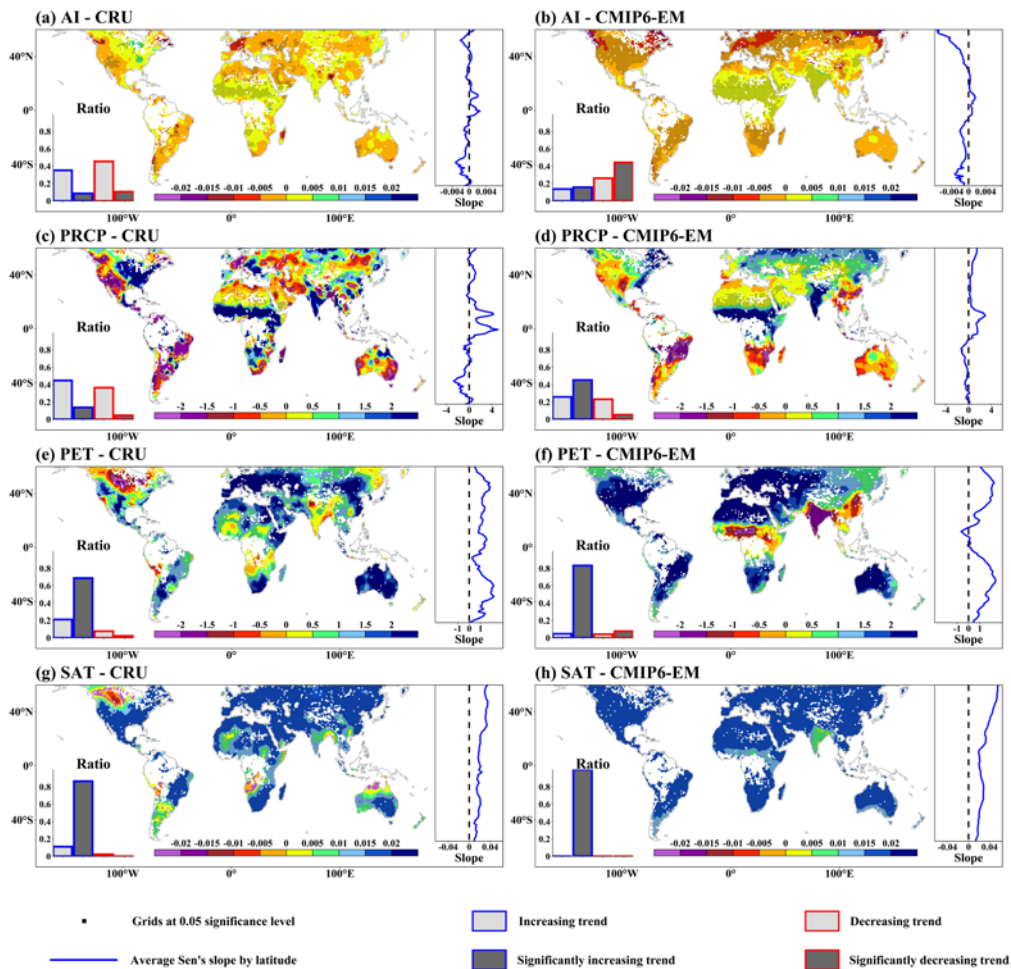


Fig. 5 The same as Fig. 4, but for annual aridity index (AI), annual precipitation (PRCP, units: mm/year), annual potential evapotranspiration (PET, units: mm/year) and annual surface air temperature (SAT, units: °C/year) using CRU data (left column) and CMIP6-EM data (right column).

To further study soil moisture variations in different climatic regions, we show soil moisture variations as a function of the climatological mean of AI (Fig. 6). Almost all climatic regions (as defined by AI) are dominated by soil moisture drying. This can be seen in all soil moisture datasets, except for the ESA CCI dataset (Fig. 6a). For the GLDAS dataset, as AI increases, the magnitude of soil moisture drying increases (Fig. 6d), indicating that wetting regions have larger drying soil moisture. However, for the GLEAM, Reanalysis, and CMIP6 datasets, the relationship between soil moisture variations and AI shows a V-shape structure (Fig. 6b, c, e, and g). Specifically, the lowest values in the V-shape structure (i.e. the most intensive drying) in regions with AI values between 0.8 and 1.2, suggest that the most prominent soil moisture drying is mainly found in humid-arid transitional regions. It should be noted that the drying peaks in the AI ranges in the GLEAM dataset are leftward relative to those in the Reanalysis and CMIP6 datasets. In these transitional regions, the magnitudes of increases in PET are relatively higher than those of increases in PRCP based on the CRU dataset (Fig. 6f). In contrast, in the CMIP6 simulations, PET and PRCP increased and decreased dramatically in the AI range of 0.8-1.2 (Fig. 6h). Under global warming, a mixed evapotranspiration regime (i.e., concurrence of water- and energy-limited evapotranspiration regimes) in the transitional regions tends to become water-limited (since there is adequate energy supplied), which turns humid areas to dry areas (Dai et al., 2013; Huang et al., 2016). Additionally, strong positive feedbacks between warming and drying can further strengthen soil moisture drying (Koster et al., 2004).

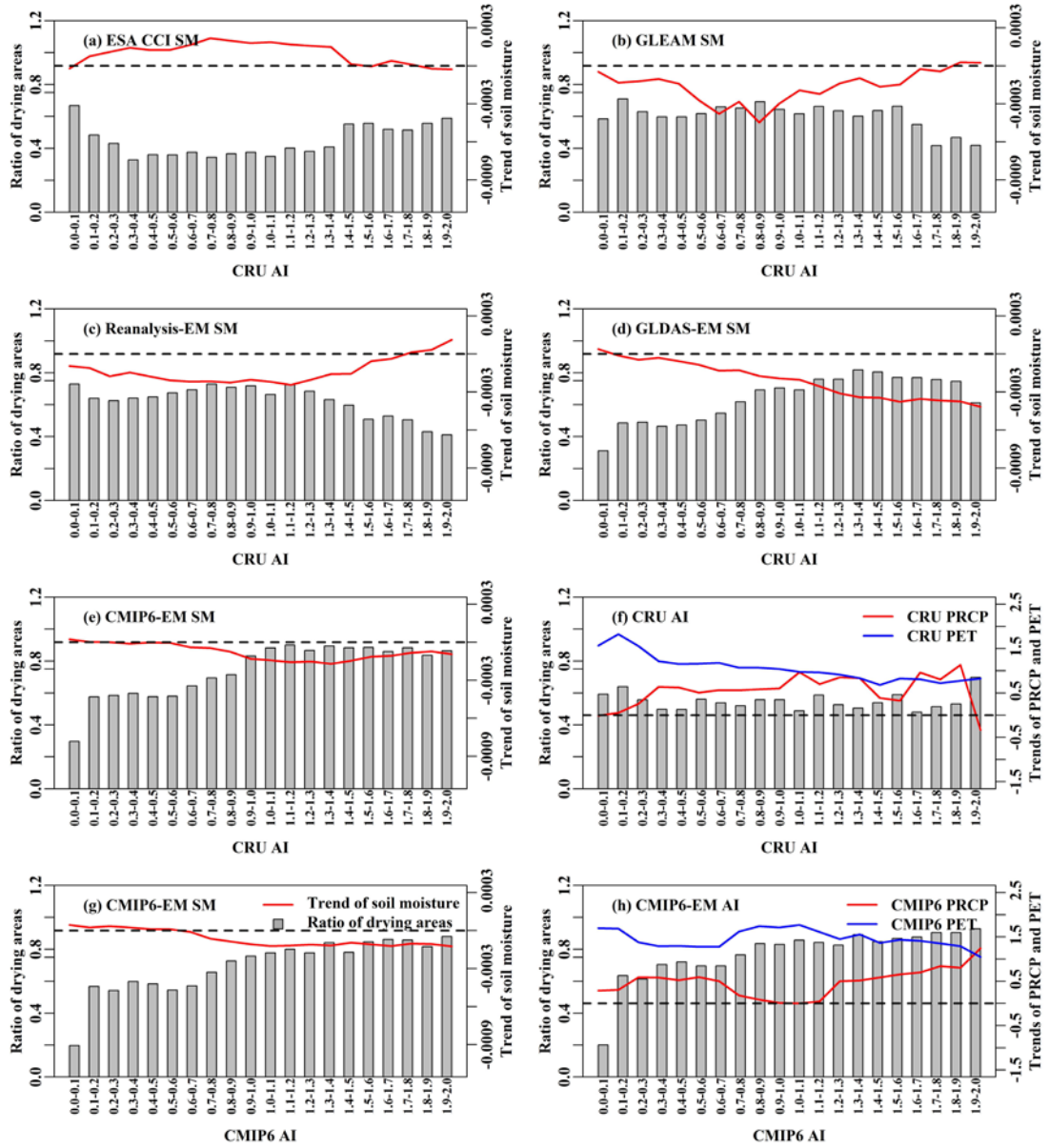


Fig. 6 (a)-(e) and (g), The Sen's slope (red line) and fraction of drying area of annual soil moisture (bar chart) as a function of the climatological mean of AI for each dataset during 1980-2020. (f) and (h), The linear trends in annual PRCP (red line), PET (blue line) and fraction of drying area defined by AI (bar chart) as a function of the long-term mean of AI.

Since PRCP and SAT jointly affect the changes in soil moisture, we analyze responses of soil moisture to changes in PRCP and SAT (Fig. 7). For all the datasets, soil moisture mostly shows drying when SAT trends are positive and PRCP trends are negative. The variations in soil moisture are due to the combined effects of changes in PRCP and SAT. However, for the ESA CCI dataset, soil moisture drying is mainly detected when the trends in PRCP are negative and the trends in SAT



are positive, while most of the wetting changes in soil moisture can be found when PRCP increases and SAT decreases. For the GLEAM, Reanalysis, and GLDAS datasets, the faster the SAT warming, the greater the soil moisture drying, implying that SAT trends play a key role in the magnitude of soil moisture drying. In the three datasets, when the positive SAT trends are very large, the soil moisture is drying, regardless of the directions of PRCP changes. In GLEAM, the warming degree determines the level of soil moisture drying when PRCP decreases, while the amplitude of PRCP increase controls the magnitude of soil moisture wetting when SAT decreases.

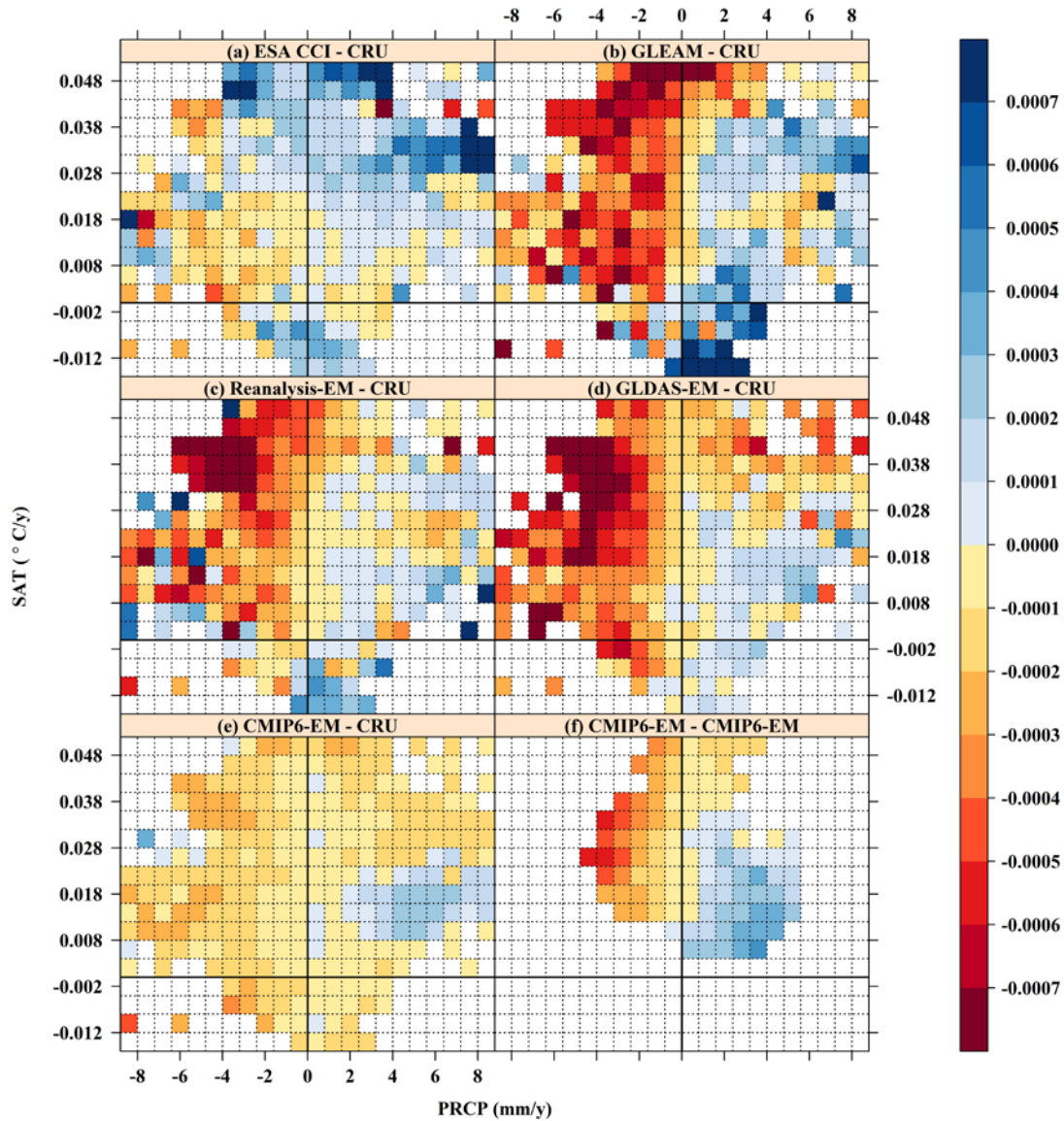


Fig. 7 Sen's slope trends in annual mean soil moisture as a function of trends in PRCP and SAT for different soil moisture datasets during 1980-2020. The colored boxes represent soil moisture trends.

The red (blue) boxes are drying (wetting), and blank indicates no data.

### **4.3 Climate drivers of variations in soil moisture**

The above inter-comparisons show different changes in soil moisture and responses of soil moisture to climatic factors among the different datasets. Here, the dynamical processes are analyzed to help interpret these differences.

First, changes in the geopotential height and wind field of 850 hPa were plotted by using the ERA5 reanalysis data (Fig. 8 left column) and the CMIP6 simulation data (Fig. 8 right column). North America is deeply affected by the westerly circulation (Wang and Ding 2006). Over the period of 1980 to 2020, the Aleutian Low has weakened with increasing geopotential height, particularly in winter (Fig. 8a-d). The weakening of the Aleutian Low and an abnormal anticyclone in the location of the Aleutian Low decelerate the westerlies along the southern flank of the Aleutian Low (Fig. 8a-h). Due to the limited transport of water vapor to North America, the deceleration of westerlies causes decreases in precipitation, thereby resulting in drying soil moisture trends in this region, which can be seen in all soil moisture datasets.

Compared with North America, East Asia and North Africa are strongly influenced by monsoon circulations, especially in the warm season. An unusual high pressure center occurs in the northeastern Asia in JJA (June-August, Fig. 8c-d), indicating a weakened land-sea low-level pressure gradient and blocking of the warm moisture transport from the Pacific Ocean to northeastern Asia. At the same time, the East Asia summer monsoon (EASM) tends to be fragile (Ueda et al., 2006; He et al., 2014), suggesting that the EASM-driven moisture struggles to reach inland and northern areas of Asia. These atmospheric circulation conditions are conducive to decreased PRCP and drying soil moisture in northeastern Asia (as seen in GLEAM, Reanalysis-EM,

GLDAS-EM, and CMIP6; Fig. 4b-e).

In the warm season, North Africa, and especially the Sahel, is strongly controlled by the West African monsoon (WAM), which carries moisture from the tropical Atlantic Ocean to the Sahel. The WAM is enhanced in the warm season, which favors transportation of moisture-rich air to the Sahel and thereby facilitates precipitation over the region (Fig. 8g-h). However, this dynamical process is only indicated by the wetting soil moisture in the Sahel in CMIP6 (Fig. 4e) and GLDAS-EM (Fig. 4d). The soil moisture wetting in the Sahel may be also explained by vegetation expansion in this region (Feng 2016). In South Africa, precipitation occurs mainly in the austral summer season. A low pressure center can be observed in southern South Africa in DJF (i.e., the austral summer season) (Fig. 8a), indicating the low-level pressure gradient between land and sea is enhanced. The accelerated easterlies from the Indian Ocean favor more moisture-rich air which results in rainfall increases and a wetting trend in southern South Africa. This process can explain the wetting trend in southern South Africa seen in most of the soil moisture datasets except CMIP6.

South America is largely affected by the typical westerly flow which transports humid air masses from the Pacific to this region. In the austral summer season, an anomalous high pressure center occurs over Patagonia (Fig. 8a), as well as anomalous easterlies along the western flank and a strong anticyclone in the west of southern South America (Fig. 8e-f). The anomalous easterlies go against the warm moisture transferred from the Pacific to southern South America, thereby favoring soil moisture drying in this region. This mechanism can explain soil moisture drying in all datasets.

In the summer season of the Southern Hemisphere, precipitation exhibits strong spatial heterogeneity across Australia, the eastern areas of which show a decreasing trend while the central and western areas exhibit an increasing trend (Wardle and Smith 2004; Shi et al. 2008). In eastern



Australia in DJF, the easterlies from the tropical western Pacific are weakened; thus, the water vapor  
 advected by the easterlies tends to be declining (Fig. 8e-f). In JJA, however, an anomalous cyclone  
 is observed over central and west Australia (Fig. 8g-h) which can carry warm moisture to the region  
 and trigger more precipitation and a wetting climate.

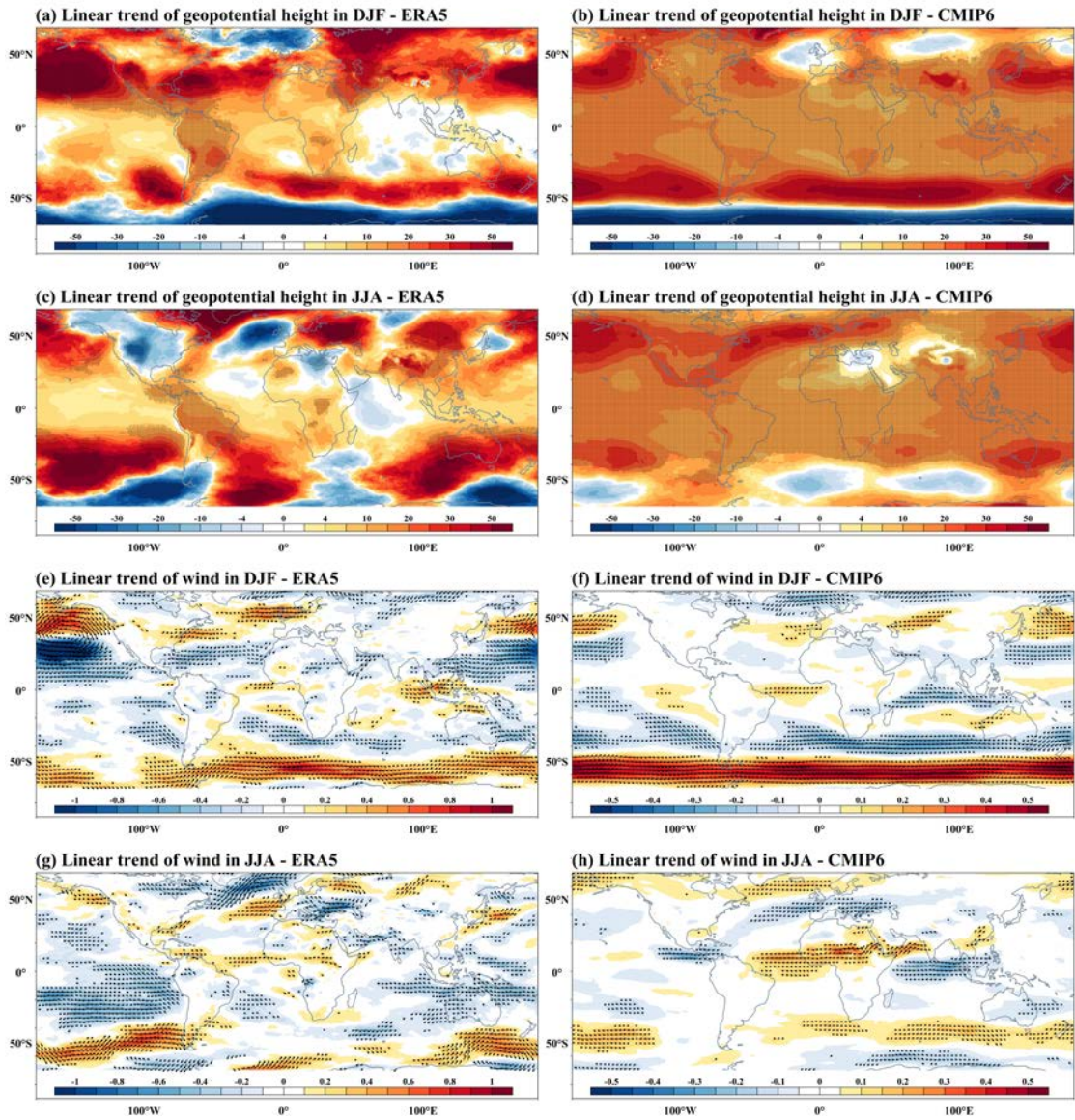


Fig. 8 Changes in large-scale environmental variables (i.e., geopotential height and wind field) during 1980-2020 using ERA5 reanalysis data (left column) and CMIP6-EM data (right column). The red (blue) regions with black points are the regions where the linear trend of geopotential height is at the 0.05 significance level based on the Mann-Kendall test.

#### 4.4 The possible influences of SST on soil moisture variations

Due to the important influence of SST on the global climate, we also discuss the impacts of SST anomalies (40°S-60°N) on soil moisture variability using MCA analysis on all datasets, with the purpose of examining whether these datasets exhibit any agreement in the relationship revealed by the leading MCA modes. In the comparison with leading MCA modes only, most of the unforced irreproducible natural variations can be excluded.

The first leading MCA mode (MCA1) can be taken as the global warming signal in soil moisture variations, because the temporal coefficients (using Spearman method) between the MCA1 of SST and SAT have strong positive correlations with values of about 0.9 in all datasets (Fig. 9), and most areas in oceans warm rapidly (Fig. S9) (Frölicher et al., 2018). The highest value of the squared fractional covariance (SFC) explained by MCA1 is 0.96 in CMIP6, and the smallest value is 0.5 in ESA CCI. Additionally, there are similar temporal evolutions of the temporal modes and the spatial patterns between MCA1 and corresponding long-term variations (Fig. 4). These results indicate the long-term changes in soil moisture can be largely explained by global warming (Fig. 9). Similarly, Dai (2013) used the MCA method to decompose SST anomalies and the Palmer drought severity index (PDSI) and identified the global warming signal represented by the first leading MCA modes. Here, we find the spatial patterns of MCA1 of the modeled datasets (i.e., GLEAM, Reanalysis-EM, GLDAS-EM and CMIP6-EM) are consistent despite some regional differences, while there is a larger discrepancy in the spatial pattern of MCA1 between ESA CCI and modeled datasets (Fig. 10). Corresponding to global warming, the spatial patterns of MCA1 show soil moisture drying in North America, Europe, northeastern Asia, and southern South America in all the datasets. Discrepancies of MCA1 can be seen in southern South Africa, Sahel, India Peninsula and Australia.

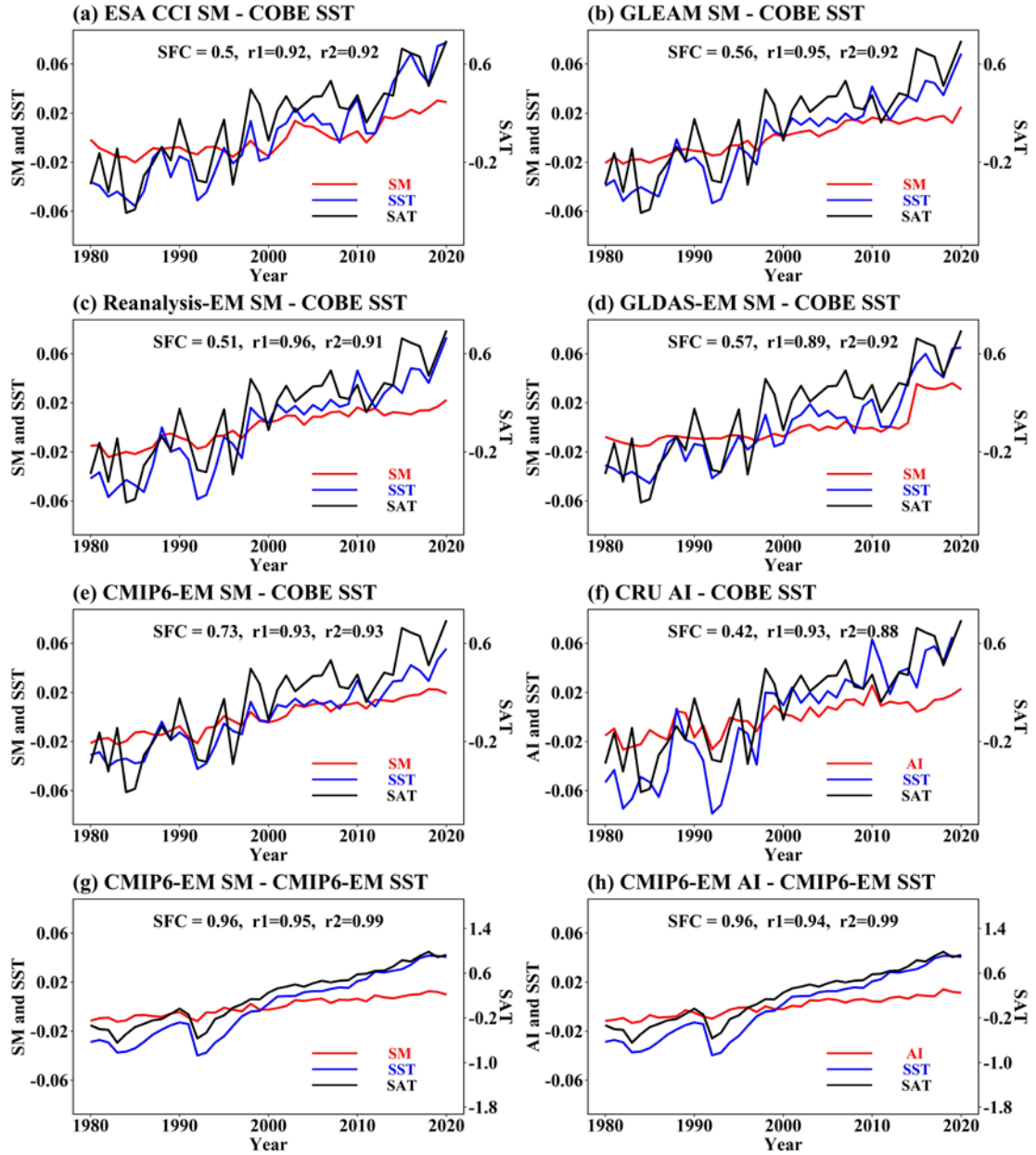


Fig. 9 Temporal changes in the first leading mode (MCA1) for sea surface temperature (SST) and soil moisture (a-e and g) and AI (f and h). The blue and red lines are temporal components of MCA1 from SST and soil moisture (a-e and g)/AI (f and h), respectively, and the black line is the global mean SAT. SFC is the squared fractional covariance explained by the MCA1 model, and r1 and r2 are the correlation coefficients between the red and blue, and blue and black lines, respectively.

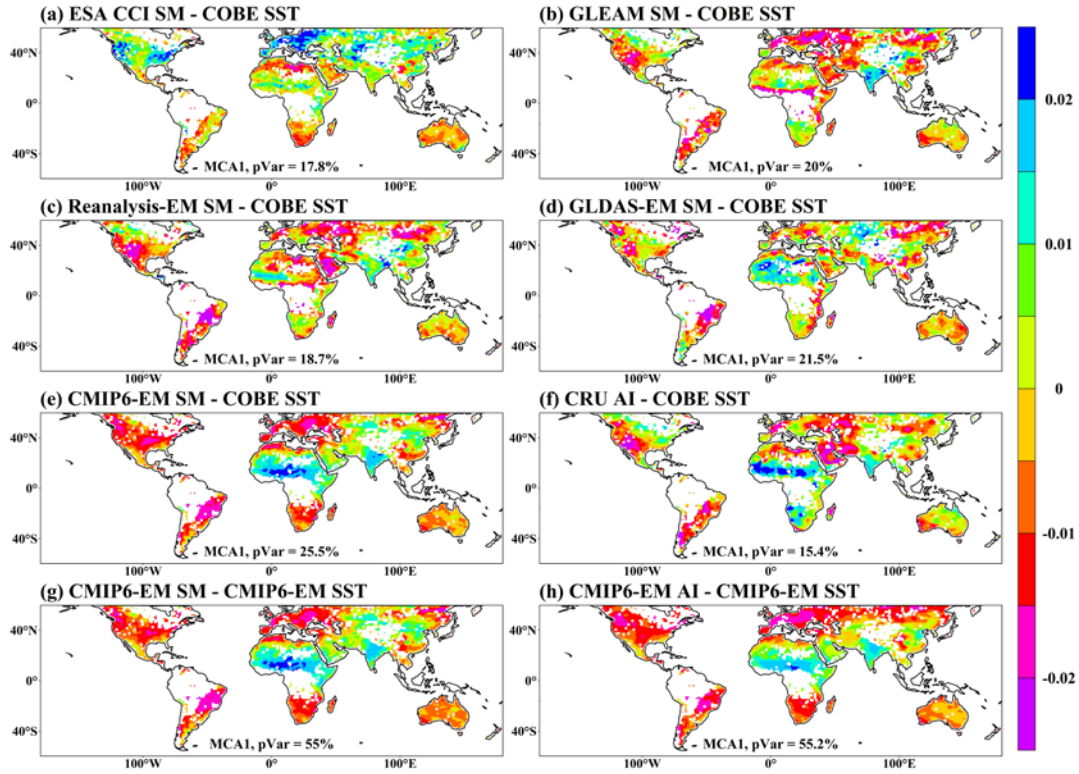


Fig. 10 Spatial patterns of the MCA1 model for soil moisture (a-e and g) and AI (f and h). pVar is the percentage variance explained by the MCA1.

We find that the second leading mode (MCA2) represents the signal of El Niño-Southern Oscillation (ENSO) in soil moisture variations, because there are high temporal coefficients (about 0.9 in all the datasets with Niño 3.4 SST) and similar spatial patterns between ENSO-induced SST and the spatial mode of SST in MCA2 (Figs. 11 and S10). Unlike the consistent increasing trends in MCA1, MCA2 in soil moisture exhibits a pattern of inter-annual variations which is similar to the fluctuation of ENSO-induced SST anomalies (Fig. 11). The spatial patterns of MCA2 are visibly different across datasets, suggesting the short-term soil moisture variability induced by ENSO depends on the selection of soil moisture dataset (Fig. 12). The patterns also exhibit weak agreement with the temporal variations of soil moisture from the corresponding datasets shown in Fig. 4.



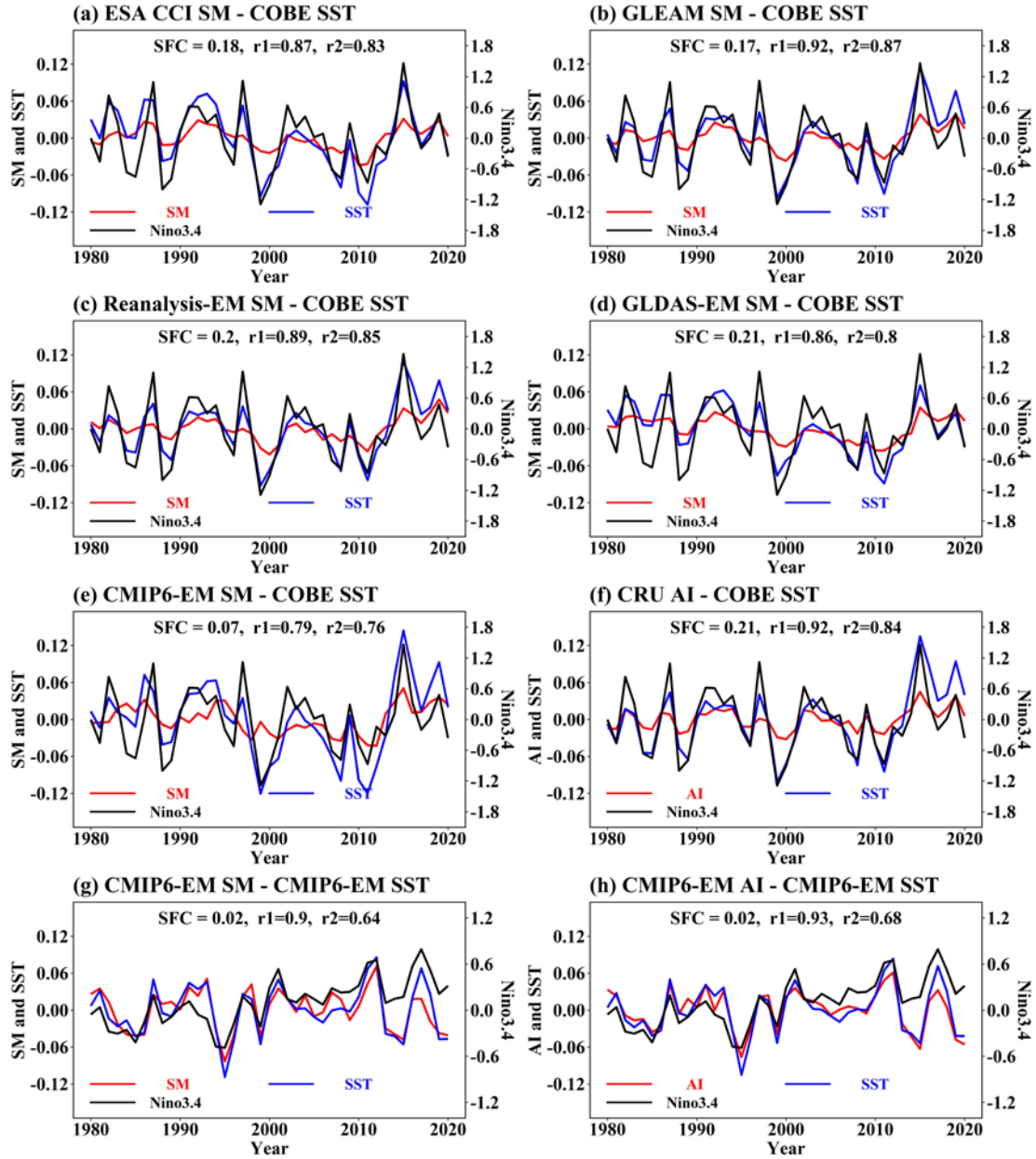


Fig. 11 The same as Fig. 9, but for the second leading mode (MCA2) and the black line is the Nino 3.4 index.

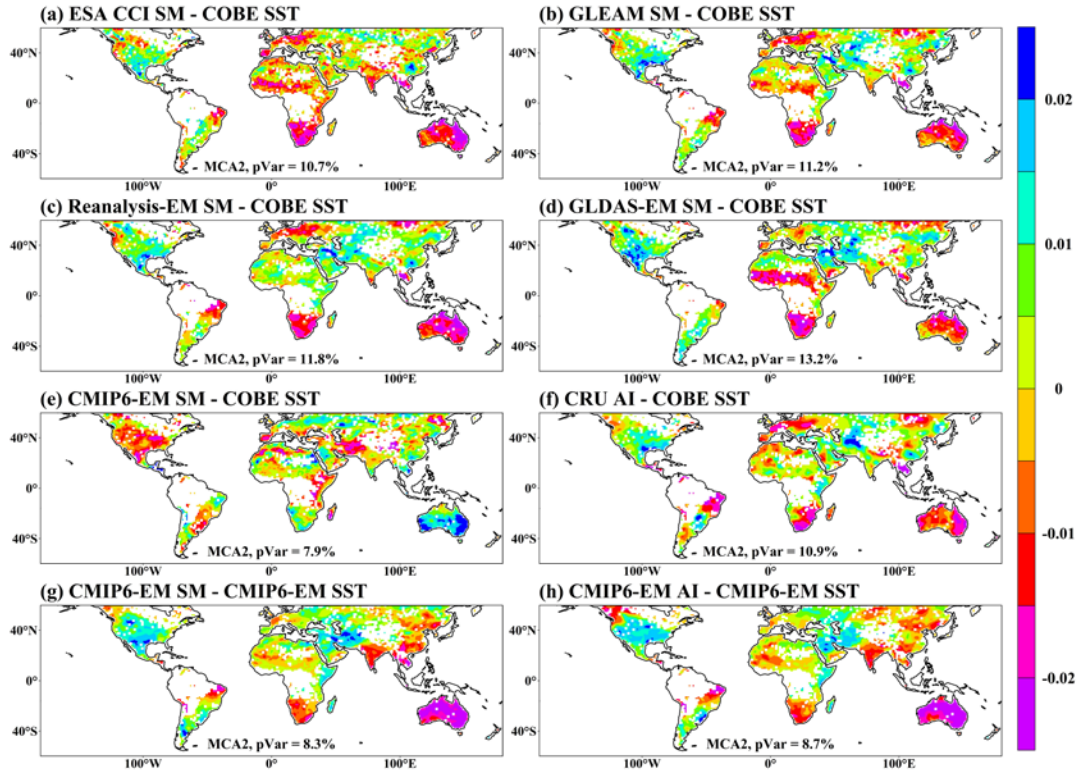


Fig. 12 The same as Fig. 10, but for MCA2.

## 5. Discussion

Our results show that in some specific regions, the spatio-temporal variations of soil moisture differ among soil moisture datasets. Here, we first discuss the possible reasons of the discrepancies in soil moisture variations in terms of temporal correlations (Figs. 2 and 3), land cover (e.g., vegetation), and human activities (e.g., irrigation). We then discuss the potential impacts of the differences in long-term variations among the datasets on investigations into the impacts of global warming on soil moisture.

Given the spatial heterogeneity in soil moisture trends (Fig. 4), we assess the soil moisture changes using regional averages (Fig. S12). Nine sub-regions are considered, following Huang et al. (2015) (Fig. S11). All datasets exhibit consistent downward variations in Europe, and South America. In North Africa, ESA CCI, GLDAS and the reanalysis datasets show the wetting trends in

soil moisture turned into drying trends in 1995, while CMIP6-based soil moisture increases continuously throughout 1980-2020. Overall, the temporal changes in regional averages of soil moisture in ESA CCI, GLEAM, Reanalysis-EM and GLDAS-EM are generally consistent with each other. The regional averages again show that CMIP6-EM can capture the direction of change of soil moisture with considerably small amplitude of temporal variations. The low variability in CMIP6 can be attributed to systematic error in the GCMs, with a lower average values of soil moisture than other datasets (Yuan and Quiring, 2017), poor ability of capturing natural variations of soil moisture (Dai, 2013), and the coarse spatial resolution. It can be seen from temporal changes in the regional averages of soil moisture for each CMIP6 model (figure not shown) that larger temporal variability of soil moisture can be found in the CMIP6 models with finer spatial resolution. In CMIP6 models with finer resolution, the soil moisture-related physical processes may be better considered in space and time, and then the spatio-temporal variability of soil moisture could be better captured.

In the GCM simulations, soil moisture is determined by meteorological forcing such as precipitation, temperature, solar radiation, soil structure, and evapotranspiration (Ruosteenoja et al., 2018). The effects of atmospheric chemistry, dynamic changes in vegetation, or other land use and land cover changes are not fully or consistently modelled (Wang et al., 2022; Gillett et al., 2016; Park et al., 2021; Ito et al., 2020). As a result, simulation biases in these factors may accumulate when modelling soil moisture, causing differences between models (Ruosteenoja et al., 2018). However, CMIP6 not only captures soil moisture trends better than CMIP5, but also has less inter-model variability (Yuan et al., 2021). The lack of full land-atmosphere feedbacks in GLEAM, GLDAS, and reanalysis datasets may be one of the reasons for the low cross-correlation between them and CMIP6 GCM simulations (Van Der Linden et al., 2020; Fig. 1).

GCMs are a commonly used tool for projecting global warming impacts on soil moisture and subsequent changes in the likelihood and intensity of drought (Dai, 2013; Chen and Sun, 2017). The small amplitude of temporal variations in soil moisture in GCMs may lead to large biases in projections of future droughts and expansion of global drylands (Feng and Fu, 2013). Although some studies have used historical data to correct the bias of GCMs projections (Huang et al., 2016), the poor agreement in the amplitude of temporal variations between CMIP6 and other datasets still underscores the challenges remaining for GCMs to adequately capture soil moisture variations.

The discrepancies in soil moisture variations between ESA CCI and the other datasets are particularly evident in East Asia (Fig. 4a), possibly due to the influence of dense vegetation and extensive irrigation. In southeastern East Asia, vegetation is expanding (Feng 2016), which mitigates the drying of soil moisture and enhances the difficulty of retrieving soil moisture (Karthikeyan et al., 2017b). In these wet areas, vegetation expansion would store more water from precipitation resulting in increases in soil moisture after evapotranspiration (Huber et al., 2011). Discrepancies in soil moisture variations between ESA CCI and simulations are observed in northern East Asia, where the irrigation is particularly intensive (Siebert et al., 2005; Shi et al., 2014). Irrigation increases soil moisture locally and largely affects local soil moisture variations (Taylor et al., 2012; Shi et al., 2014; Qiu et al., 2016). The impacts of irrigation are hard to simulate in models, but can be monitored by satellites. For example, ESA CCI captures soil moisture variations induced by irrigation in northern Asia (Qiu et al., 2016).

These discrepancies in temporal variations among the datasets imply that the assessment of soil moisture changes under global warming is highly dependent on the choice of soil moisture dataset. Therefore, we employ multiple datasets to analyze the response of soil moisture changes to



global warming. We show the mode representing global warming can be extracted from all soil moisture datasets by using the MCA method (Fig. 9). This result is in line with previous studies which identified an anthropogenic signal in global soil moisture drying based on just one or two types of soil moisture datasets (Dai, 2013; Gu et al., 2019c; Marvel et al., 2019). For example, Marvel et al. (2019) used an empirical orthogonal function to extract the “fingerprint” of anthropogenic warming from the PDSI as well as CMIP5 soil moisture, indicating that the signal of greenhouse gas forcing is present in soil moisture variations from 1981 to the present. Using GLDAS and CMIP5 datasets, Gu et al. (2019c) quantified the contributions of anthropogenic warming to global soil moisture drying (i.e.,  $2.1 \times 10^{-3} \text{ m}^3/\text{m}^3$  over 1948-2005). Our results suggest that using only one or two types of soil moisture datasets, as in previous studies, may be insufficient. Our findings further indicate that the spatial patterns of soil moisture response to global warming are consistent among the different types of datasets used in this study.

## 6. Summary and conclusions

We analyze and compare the spatio-temporal variations of soil moisture over 1980 to 2020 from a wide range of datasets, including ESA CCI, GLEAM, Reanalysis-EM, GLDAS-EM and CMIP6 GCMs. We analyze the relations between soil moisture variations and climatic drivers including PRCP and SAT. The similarities and differences in the long-term variations and the relations among different datasets are also discussed.

The ESA CCI, GLEAM, Reanalysis-EM, and GLDAS-EM datasets exhibit high similarity in annual mean soil moisture. Significant positive correlations among the datasets are mainly detected in southern South America, North America, Australia, and northeastern Asia. In terms of the long-

term trends, most of the datasets agree on widespread global soil moisture drying with prominent drying in North America, Europe, northeastern Asia, North Africa, and the Arabian Peninsula, despite inconsistencies in the magnitude of trends and regional differences among the datasets. The most intensive drying of soil moisture occurs in the humid-arid transitional regions (with an AI index of 0.8-1.2) where the proportion of drying areas is also the highest. The variations of soil moisture can be explained by dynamical processes (circulation, monsoon, and water vapor transport), particularly in North America, northeastern Asia, southern South America, and southern South Africa.

Trends in precipitation have a limited influence on the trends in soil moisture in the GLEAM, reanalysis, GLDAS, and CMIP6 datasets, because soil moisture usually tends to dry when temperature increases, regardless of the changes in precipitation. On the other hand, in ESA CCI and GLEAM, the impacts of precipitation on the variations in soil moisture are substantial. Overall, most of the datasets, and especially GLEAM, reveal strong effects of changes in temperature on the changes in soil moisture. The dominant role of temperature changes is further supported by the MCA1 in soil moisture variations, which mainly shows the impacts of global warming. The MCA2, in contrast, mainly represents the influence of ENSO, and shows that short-term ENSO-induced variabilities are sensitive to the selection of datasets .

**CRedit authorship contribution statement:** **Yansong Guan:** Methodology, Software, Visualization. **Xihui Gu:** Formal analysis, Investigation, Conceptualization, Data curation, Funding acquisition, Project administration, Resources, Supervision, Validation, Writing – original draft, Writing – review & editing. **Jianfeng Li:** Conceptualization, Funding acquisition, Project

administration, Writing – review & editing. **Dongdong Kong:** Writing – review & editing. **Xiang Zhang:** Writing – review & editing. **Louise J. Slater:** Writing – review & editing.

**Declaration of Competing Interest:** The authors declare that they have no known competing financial interests or personal relationships that could have influenced the work reported in this paper.

**Acknowledgments:** This work has been funded by the National Key R&D Program of China (Grant 2023YFE0103900), the National Natural Science Foundation of China (Grant No. 41901041), the open funding from Key Laboratory of Meteorological Disaster Ministry of Education & Collaborative Innovation Center on Forecast and Evaluation of Meteorological Disasters, Nanjing University of Information Science & Technology (Grant KLME202308), the open funding from the Institute of Arid Meteorology, China Meteorological Administration, Lanzhou (Grant IAM202214), the Belt and Road Special Foundation of the National Key Laboratory of Water Disaster Prevention (Grant 2022nkms03), the Pre-research Project of SongShan Laboratory (Grant YYYY062022001), the fund for State Key Laboratory of Loess and Quaternary Geology, Institute of Earth Environment (Grant No. SKLLQG2108), and the grants from the Research Grants Council of the Hong Kong Special Administrative Region (Project Nos. HKBU22301916 and HKBU12302518). Xihui Gu is supported by the China Scholarship Council.

**Data availability:** All the datasets used in this study are publicly available (see Tables 1-3 for the URLs).

638

639 **References**

- 640 Albergel, C., de Rosnay, P., Gruhier, C., Muñoz-Sabater, J., Hasenauer, S., Isaksen, L., Kerr, Y.,  
641 Wagner, W. (2012). Evaluation of remotely sensed and modelled soil moisture products using  
642 global ground-based in situ observations. *Remote Sensing of Environment*, 118, 215-226.  
643 <https://doi.org/10.1016/j.rse.2011.11.017>
- 644 Allen, R. G., Pereira, L. S., Raes, D., Smith, M. (1998). Crop evapotranspiration}Guidelines for  
645 computing crop water requirements. *FAO Irrigation and Drainage Paper 56, Food and*  
646 *Agriculture Organization of the United Nations*, 300 pp.  
647 <http://www.fao.org/docrep/X0490E/X0490E00.htm>
- 648 Barriopedro, D., Fischer, E. M., Luterbacher, J., Trigo, R. M., Garcia-Herrera, R. (2011). The hot  
649 summer of 2010: Redrawing the temperature record map of Europe. *Science*, 332(6026), 220–  
650 224. <https://doi.org/10.1126/science.1201224>
- 651 Baik, J., Zohaib, M., Kim, U., Aadil, M., Choi, M. (2019). Agricultural drought assessment based  
652 on multiple soil moisture products. *Journal of Arid Environments*, 167, 43–55.  
653 <https://doi.org/10.1016/j.jaridenv.2019.04.007>
- 654 Bi, H., Ma, J., Zheng, W., Zeng, J. (2016). Comparison of soil moisture in GLDAS model  
655 simulations and in situ observations over the Tibetan Plateau. *Journal of Geophysical Research:*  
656 *Atmospheres*, 121, 2658–2678. <https://doi.org/10.1002/2015JD024131>
- 657 Biasutti, M. (2019). Rainfall trends in the African Sahel: Characteristics, processes, and causes.  
658 *WIREs Climate Change*, 10, e591. <https://doi.org/10.1002/wcc.591>
- 659 Botter, G., Peratoner, F., Porporato, A., Rodriguez, I. I., Rinaldo, A. (2007). Signatures of large scale

660 soil moisture dynamics on streamflow statistics across US climate regimes. *Water Resources*  
661 *Research*, 43, W11413. <https://doi.org/10.1029/2007WR006162>

662 Brunner, M.I., Swain, D.L., Wood, R.R. et al. (2021). An extremeness threshold determines the  
663 regional response of floods to changes in rainfall extremes. *Communications Earth &*  
664 *Environment*, 2, 173. <https://doi.org/10.1038/s43247-021-00248-x>

665 Cammalleri, C., Vogt, J.V., Bisselink, B., De Roo, A. (2017). Comparing soil moisture anomalies  
666 from multiple independent sources over different regions across the globe. *Hydrology and*  
667 *Earth System Sciences*, 21, 6329–6343. <https://doi.org/10.5194/hess-21-6329-2017>

668 Chen, Y., Yang, K., Qin, J., Zhao, L., Tang, W., Han, M. (2013). Evaluation of AMSR-E retrievals  
669 and GLDAS simulations against observations of a soil moisture network on the central Tibetan  
670 Plateau. *Journal of Geophysical Research: Atmospheres*, 118, 4466–4475.  
671 <https://doi.org/10.1002/jgrd.50301>

672 Chen, X., Su, Y., Liao, J., Shang, J., Dong, T., Wang, C., Liu, W., Zhou, G., Liu, L. (2016). Detecting  
673 significant decreasing trends of land surface soil moisture in eastern China during the past three  
674 decades (1979–2010). *Journal of Geophysical Research: Atmospheres*, 121, 5177–5192.  
675 <https://doi.org/10.1002/2015JD024676>

676 Chen, H., Sun, J. (2017). Anthropogenic warming has caused hot droughts more frequently in China.  
677 *Journal of Hydrology*, 544, 306–318. <https://doi.org/10.1016/j.jhydrol.2016.11.044>

678 Cheng, S., Guan, X., Huang, J., Ji, F., Guo, R. (2015). Long-term trend and variability of soil  
679 moisture over East Asia. *Journal of Geophysical Research: Atmospheres*, 120, 8658–8670.  
680 <https://doi.org/10.1002/2015JD023206>

681 Cheng, S., Huang, J. (2016). Enhanced soil moisture drying in transitional regions under a warming

climate. *Journal of Geophysical Research: Atmospheres*, 121, 2542-2555.

<https://doi.org/10.1002/2015JD024559>

Dai, A. (2013). Increasing drought under global warming in observations and models. *Nature Climate Change*, 3, 52-58. <https://doi.org/10.1038/NCLIMATE1633>

Das, K., Singh, J., Hazra, J. (2019). Comparison of Smap, Gldas and Simulated Soil Moisture Datasets Over A Malaysian Region, in: IGARSS 2019 - 2019 IEEE International Geoscience and Remote Sensing Symposium. Presented at the IGARSS 2019 - 2019 IEEE International Geoscience and Remote Sensing Symposium, IEEE, Yokohama, Japan, pp. 6298–6301. <https://doi.org/10.1109/IGARSS.2019.8900589>

Deng, Y., Wang, S., Bai, X., Luo, G., Wu, L., Cao, Y., Li, H., Li, C., Yang, Y., Hu, Z., Tian, S. (2020). Variation trend of global soil moisture and its cause analysis. *Ecological Indicators*. 110, 105939. <https://doi.org/10.1016/j.ecolind.2019.105939>

Dorigo, W., Jeu, R., Chung, D., Parinussa, R., Liu, Y., Wagner, W., Fernández-Prieto, D. (2012). Evaluating global trends (1988–2010) in harmonized multi-satellite surface soil moisture. *Geophysical Research Letters*, 39, L18405. <https://doi.org/10.1029/2012GL052988>

Dorigo, W. A., Gruber, A., De Jeu, R. A. M., Wagner, W., Stacke, T., Loew, A., Albergel, C., Brocca, L., Chung, D., Parinussa, R. M., Kidd, R. (2015). Evaluation of the ESA CCI soil moisture product using ground-based observations. *Remote Sensing of Environment*, 162, 380-395. <http://dx.doi.org/10.1016/j.rse.2014.07.023>

Dorigo, W.A., Wagner, W., Albergel, C., Albrecht, F., Balsamo, G., Brocca, L., Chung, D., Ertl, M., Forkel, M., Gruber, A., Haas, E., Hamer, D. P. Hirschi, M., Ikonen, J., De Jeu, R. Kidd, R. Lahoz, W., Liu, Y.Y., Miralles, D., Lecomte, P. (2017). ESA CCI Soil Moisture for improved

704 Earth system understanding: State-of-the art and future directions. *Remote Sensing of*  
705 *Environment*, 203, 185-215. <https://doi.org/10.1016/j.rse.2017.07.001>

706 Dorigo, W., Wagner, W., Gruber, A., Scanlon, T., Hahn, S., Kidd, R., Paulik, C., Reimer, C., Van der  
707 Schalie, R., Preimesberger, W., De Jeu, R. (2019). ESA Soil Moisture Climate Change Initiative  
708 (Soil\_Moisture\_cci): Version 04.4 data collection. *Centre for Environmental Data Analysis*, 06  
709 May 2019. <http://dx.doi.org/10.5285/dce27a397eaf47e797050c220972ca0e>

710 Escorihuela, M.J., Quintana-Seguí, P. (2016). Comparison of remote sensing and simulated soil  
711 moisture datasets in Mediterranean landscapes. *Remote Sensing of Environment*, 180, 99–114.  
712 <https://doi.org/10.1016/j.rse.2016.02.046>

713 Elliott, J., Deryng, D., Müller, C. (2014). Constraints and potentials of future irrigation water  
714 availability on agricultural production under climate change. *Proceedings of the National*  
715 *Academy of Sciences of the United States of America*, 111, 3239–3244.  
716 <http://dx.doi.org/10.1073/pnas.1222474110>

717 Entekhabi, D., Njoku, E. G., Neill, P. E., Kellogg, K. H., Crow, W. T., Edelstein, W. N., Entin, J. K.,  
718 Goodman, S. D., Jackson, T. J., Johnson, J., Kimball, J., Piepmeier, J. R., Koster, R. D., Martin,  
719 N., McDonald, K. C., Moghaddam, M., Moran, S., Reichle, R., Shi, J. C., Spencer, M. W.,  
720 Thurman, S. W., Tsang, L., Zyl, J. V. (2010). The soil moisture active passive (SMAP) mission.  
721 *Proceedings of the IEEE*, 98, 704–716. <http://dx.doi.org/10.1109/JPROC.2010.2043918>

722 Eyring, V., Bony, S., Meehl, G. A., Senior, C. A., Stevens, B., Stouffer, R. J., Taylor, K. E. (2016).  
723 Overview of the Coupled Model Intercomparison Project Phase 6 (CMIP6) experimental  
724 design and organization, *Geoscientific Model Development*, 9, 1937–1958.  
725 <https://doi.org/10.5194/gmd-9-1937-2016>.

726 Feng, H. (2016). Individual contributions of climate and vegetation change to soil moisture trends  
727 across multiple spatial scales. *Scientific Reports*, 6, 32728.  
728 <http://dx.doi.org/10.1038/srep32782>

729 Feng, S., Fu, Q. (2013). Expansion of global drylands under a warming climate. *Atmospheric*  
730 *Chemistry and Physics*, 13, 10081-10094. <http://dx.doi.org/10.5194/acp-13-10081-2013>

731 Feng, S., Gu, X., Luo, S., Liu, R., Gulakhmadov, A., Slater, L. J., Li, J., Zhang, X., Kong, D. (2022).  
732 Greenhouse gas emissions drive global dryland expansion but not spatial patterns of change in  
733 aridification. *Journal of Climate*, 35, 2901-2917. <https://doi.org/10.1175/JCLI-D-22-0103.1>

734 Ford, T. W., Rapp, A. D., Quiring, S. M., Blake, J. (2015). Soil moisture–precipitation coupling:  
735 observations from the Oklahoma Mesonet and underlying physical mechanisms. *Hydrology*  
736 *and Earth System Sciences*, 19, 3617–3631. <http://dx.doi.org/10.5194/hess-19-3617-2015>

737 Frölicher, T. L., Fischer, E. M., Gruber, N. (2018). Marine heatwaves under global warming. *Nature*,  
738 560, 360-364. <https://doi.org/10.1038/s41586-018-0383-9>

739 Gelaro, R., Mccarty, W., Suarez, M.J., Todling, R., Molod, A., Takacs, L., Randles, C.A., Darmenov,  
740 A., Bosilovich, M.G., Reichle, R., Wargan, K., Coy, L., Cullather, R., Draper, C., Akella,  
741 S., Buchard, V., Conaty, A., Da Silva, A.M., Gu, W., Kim, G.-K., Koster, R., Lucchesi,  
742 R., Merkova, D., Nielsen, J.E., Partyka, G., Pawson, S., Putman, W., Rienecker, M., Schubert,  
743 S.D., Sienkiewicz, M. and Zhao, B. (2017). The modern-era retrospective analysis for research  
744 and applications, version 2 (MERRA-2). *Journal of Climate*, 30, 5419–  
745 5454. <https://doi.org/10.1175/JCLI-D-16-0758.1>.

746 Gillett, N.P., Shiogama, H., Funke, B., Hegerl, G., Knutti, R., Matthes, K., Santer, B.D., Stone, D.,  
747 Tebaldi, C. (2016). The Detection and Attribution Model Intercomparison Project (DAMIP



748 v1.0) contribution to CMIP6. *Geoscientific Model Development*, 9, 3685–3697.

749 <https://doi.org/10.5194/gmd-9-3685-2016>

750 Gruber, A., Dorigo, W. A., Crow, W., Wagner W. (2017). Triple Collocation-Based Merging of

751 Satellite Soil Moisture Retrievals. *IEEE Transactions on Geoscience and Remote Sensing*, 55,

752 6780-6792. <https://doi.org/10.1109/TGRS.2017.2734070>

753 Gruber, A., Scanlon, T., van der Schalie, R., Wagner, W., Dorigo, W. (2019). Evolution of the ESA

754 CCI Soil Moisture climate data records and their underlying merging methodology. *Earth*

755 *System Science Data*, 11, 717-739. <https://doi.org/10.5194/essd-11-717-2019>

756 Gu, X., Zhang, Q., Singh, V. P., Xiao, M., Chen, J. (2017a). Nonstationarity-based evaluation of

757 flood risk in the Pearl River basin: changing patterns, causes and implications. *Hydrological*

758 *Sciences Journal*, 62, 246-258. <https://doi.org/10.1080/02626667.2016.1183774>

759 Gu, X., Zhang, Q., Singh, V. P., Liu, L., Shi, P. (2017b). Spatiotemporal patterns of annual and

760 seasonal precipitation extreme distributions across China and potential impact of tropical

761 cyclones. *International Journal of Climatology*, 37, 3949-3962.

762 <https://doi.org/10.1002/joc.4969>

763 Gu, X., Zhang, Q., Singh, V. P., Shi, P. (2017c). Changes in magnitude and frequency of heavy

764 precipitation across China and its potential links to summer temperature. *Journal of Hydrology*,

765 547, 718-731. <https://doi.org/10.1016/j.jhydrol.2017.02.041>

766 Gu, X., Zhang, Q., Li, J., Singh, V. P., Liu, J., Sun, P., et al. (2019a). Intensification and expansion

767 of soil moisture drying in warm season over Eurasia under global warming. *Journal of*

768 *Geophysical Research: Atmospheres*, 124. <https://doi.org/10.1029/2018JD029776>

769 Gu, X., Li, J., Chen, Y. D., Kong, D., & Liu, J. (2019b). Consistency and discrepancy of global

surface soil moisture changes from multiple model - based data sets against satellite observations. *Journal of Geophysical Research: Atmospheres*, 124. <https://doi.org/10.1029/2018JD029304>

Gu, X., Zhang, Q., Li, J., Singh, V. P., Liu, J., Sun, P., Cheng, C. (2019c). Attribution of global soil moisture drying to human activities: A quantitative viewpoint. *Geophysical Research Letters*, 46, 2573-2582. <https://doi.org/10.1029/2018GL080768>

Guan, Y., Gu, X., Slater, L. J., Li, L., Kong, D., Liu, J., Zhang, X., Yan, X. (2022). Tracing anomalies in moisture recycling and transport to two record-breaking droughts over the Mid-to-Lower Reaches of the Yangtze River. *Journal of Hydrology*, 609, 127787. <https://doi.org/10.1016/j.jhydrol.2022.127787>

Harris, I., Osborn, T.J., Jones, P., Lister, D. (2020). Version 4 of the CRU TS monthly high-resolution gridded multivariate climate dataset. *Scientific Data*, 7, 109. <https://doi.org/10.1038/s41597-020-0453-3>

Hauser, M., Orth, R., Seneviratne, S. I. (2016). Role of soil moisture versus recent climate change for the 2010 heat wave in Russia. *Geophysical Research Letters*, 43, 2819–2826. <https://doi.org/10.1002/2016GL068036>

Hirschi, M., Seneviratne, S. L., Alexandrov, V., Boberg, F., Boroneant, C., Christensen, O. B., Formayer, H., Orłowsky, B., Stepanek, P. (2010). Observational evidence for soil-moisture impact on hot extremes in southeastern Europe. *Nature Geoscience*, 4, 17-21. <https://doi.org/10.1038/NGEO1032>

Hoffmann, L., et al. (2019). From ERA-Interim to ERA5: the considerable impact of ECMWF's next-generation reanalysis on Lagrangian transport simulations. *Atmospheric Chemistry and*

792        *Physics*, 19, 3097-3124. <https://doi.org/10.5194/acp-19-3097-2019>

793        Holgate, C.M., De Jeu, R.A.M., Van Dijk, A.I.J.M., Liu, Y.Y., Renzullo, L.J., Vinodkumar, Dharssi,

794        I., Parinussa, R.M., Van Der Schalie, R., Gevaert, A., Walker, J., McJannet, D., Cleverly, J.,

795        Haverd, V., Trudinger, C.M., Briggs, P.R. (2016). Comparison of remotely sensed and modelled

796        soil moisture data sets across Australia. *Remote Sensing of Environment*, 186, 479–500.

797        <https://doi.org/10.1016/j.rse.2016.09.015>

798        Huang, J., Li, M., Xie, Y., Wang, S., Ye, H., Ran, J. (2015). Global semi-arid climate change over

799        last 60 years. *Climate Dynamics*, 46, 1131-1150. <https://doi.org/10.1007/s00382-015-2636-8>

800        Huang, J., Yu, H., Guan, X., Wang, G., Guo, R. (2016). Accelerated dryland expansion under climate

801        change. *Nature Climate Change*, 6, 166-171. <https://doi.org/10.1038/NCLIMATE2837>

802        Huber, S., Fensholt, R., Rasmussen, K. (2011). Water availability as the driver of vegetation

803        dynamics in the African Sahel from 1982 to 2007. *Global and Planetary Change*, 76, 186-195.

804        <https://doi.org/10.1016/j.gloplacha.2011.01.006>

805        Humphrey, V., Berg, A., Ciais, P. et al. (2021). Soil moisture–atmosphere feedback dominates land

806        carbon uptake variability. *Nature*, 592, 65–69. <https://doi.org/10.1038/s41586-021-03325-5>

807        IPCC (2014). Climate Change 2014: Synthesis Report. Contribution of Working Groups I, II and III

808        to the Fifth Assessment Report of the Intergovernmental Panel on Climate Change [Core

809        Writing Team, R.K. Pachauri and L.A. Meyer (eds.)]. IPCC, Geneva, Switzerland.

810        Ishii, M. A., Shouji, S., Sugimoto, S., Matsumoto, T. (2005). Objective analyzes of sea-surface

811        temperature and marine meteorological variables for the 20th century using ICOADS and the

812        Kobe collection. *International Journal of Climatology*, 25, 865-879.

813        <https://doi.org/10.1002/joc.1169>

814 Ito, A., Hajima, T., Lawrence, D.M., Brovkin, V., Delire, C., Guenet, B., Jones, C.D., Malyshev, S.,  
815 Materia, S., McDermid, S.P., Peano, D., Pongratz, J., Robertson, E., Shevliakova, E., Vuichard,  
816 N., Wårlind, D., Wiltshire, A., Ziehn, T. (2020). Soil carbon sequestration simulated in CMIP6-  
817 LUMIP models: implications for climatic mitigation. *Environmental Research Letters*, 15,  
818 124061. <https://doi.org/10.1088/1748-9326/abc912>

819 Jiang, K., Pan, Z., Pan, F., Wang, J., Han, G., Song, Y., Zhang, Z., Huang, N., Ma, S., Chen, X.  
820 (2022). Influence patterns of soil moisture change on surface-air temperature difference under  
821 different climatic background. *Science of The Total Environment*, 822, 153607.  
822 <https://doi.org/10.1016/j.scitotenv.2022.153607>

823 Karthikeyan, L., Pan, M., Wanders, N., Kumar, D. N., Wood, E. F. (2017a). Four decades of  
824 microwave satellite soil moisture observations: Part 2. Product validation and inter-satellite  
825 comparisons. *Advance in Water Resources*, 109, 236-252.  
826 <http://dx.doi.org/10.1016/j.advwatres.2017.09.010>

827 Karthikeyan, L., Pan, M., Wanders, N., Kumar, D. N., Wood, E. F. (2017b). Four decades of  
828 microwave satellite soil moisture observations: Part 1. A review of retrieval algorithms.  
829 *Advance in Water Resources*, 109, 106-120.  
830 <http://dx.doi.org/10.1016/j.advwatres.2017.09.006>

831 Kendall, M. G. (1975). Rank Correlation Methods. Griffin: London.

832 Kerr, Y. H., Waldteufel, P., Wigneron, J. P., Delwart, S., Cabot, F. O., Boutin, J., Escorihuela, M.-J.,  
833 Font, J., Reul, N., Gruhier, C., Juglea, S. E., Drinkwater, M. R., Hahne, A., Martin-Neira, M.,  
834 Mecklenburg, S. (2010). The SMOS mission: New tool for monitoring key elements of the  
835 global water cycle. *Proceedings of the IEEE*, 98, 666–687.

836 <http://dx.doi.org/10.1109/JPROC.2010.2043032>

837 Knutti, R., Sedlace, J. (2013). Robustness and uncertainties in the new CMIP5 climate model  
838 projections. *Nature Climate Change*, 3, 369-373. <http://dx.doi.org/10.1038/NCLIMATE1716>

839 Kong, D., McVicar, T., Xiao, M., Zhang, Y., Peña-Arancibia, J., Filippa, G., Xie, Y., Gu, X. (2022).  
840 phenofit: An R package for extracting vegetation phenology from time series remote sensing.  
841 *Methods in Ecology and Evolution*, 13, 1508-1527. <https://doi.org/10.1111/2041-210X.13870>

842 Koster, R. D., et al. (2004). Regions of Strong coupling between soil moisture and precipitation.  
843 *Science*, 305(5687), 1138-1140. <http://dx.doi.org/10.1126/science.1100217>

844 Jiang, K., Pan, Z., Pan, F., Wang, J., Han, G., Song, Y., Zhang, Z., Huang, N., Ma, S., Chen, X.  
845 (2022). Influence patterns of soil moisture change on surface-air temperature difference under  
846 different climatic background. *Science of The Total Environment*, 822, 153607.  
847 <https://doi.org/10.1016/j.scitotenv.2022.153607>

848 Leonardi, A. P., Morey, S. L., O'Brien, J. J. (2002). Interannual variability in the eastern subtropical  
849 North Pacific Ocean. *Journal of Physical Oceanography*, 32, 1824–1837.  
850 [https://doi.org/10.1175/1520-0485\(2002\)032<1824:IVITES>2.0.CO;2](https://doi.org/10.1175/1520-0485(2002)032<1824:IVITES>2.0.CO;2)

851 Li, H., Ye, A., Zhang, Y., Zhao, W. (2021). InterComparison and Evaluation of MultiSource Soil  
852 Moisture Products in China. *Earth and Space Science*, 8.  
853 <https://doi.org/10.1029/2021EA001845>

854 Li, J., Chen, Y. D., Gan, T. Y., Lau, N.-C. (2018). Elevated increases in human-perceived  
855 temperature under climate warming. *Nature Climate Change*, 8, 43-47.  
856 <https://doi.org/10.1038/s41558-017-0036-2>

857 Li, J. P., Zeng, Q. C. (2002). A unified monsoon index. *Geophysical Research Letters*, 29(8), 1274.

858 <https://doi.org/10.1029/2001GL013874>

859 Li, M, Wu, P, Ma, Z. (2020). A comprehensive evaluation of soil moisture and soil temperature from  
860 third-generation atmospheric and land reanalysis data sets. *International Journal of*  
861 *Climatology*, 40, 5744-5766. <https://doi.org/10.1002/joc.6549>

862 Li, M., Wu, P., Sexton, D.M.H., Ma, Z. (2021). Potential shifts in climate zones under a future global  
863 warming scenario using soil moisture classification. *Climate Dynamics*, 56, 2071-2092.  
864 <https://doi.org/10.1007/s00382-020-05576-w>

865 Lin, B., Stackhouse, P. W., Minnis, P., Wielicki, B. A., Hu, Y., Sun, W., Fan, T. F., Hinkelman, L. M.  
866 (2008). Assessment of global annual atmospheric energy balance from satellite observations.  
867 *Journal of Geophysical Research: Atmospheres*, 113, D16114.  
868 <https://doi.org/10.1029/2008JD009869>

869 Liu, Y. Y., et al. (2011). Developing an improved soil moisture dataset by blending passive and  
870 active microwave satellite-based retrievals. *Hydrology and Earth System Sciences*, 15, 425–  
871 436. <https://doi.org/10.5194/hess-15-425-2011>

872 Liu, Y. Y., et al. (2012). Trend-preserving blending of passive and active microwave soil moisture  
873 retrievals. *Remote Sensing of Environment*, 123, 280–297.  
874 <https://doi.org/10.1016/j.rse.2012.03.014>

875 Liu, Z., Wang, Y., Wang, Y., et al. (2021). Separating meteorological condition and soil moisture  
876 controls on the variation in stand evapotranspiration of a larch plantation during three  
877 hydrological years. *Global Ecology and Conservation*, 27, e01548.  
878 <https://doi.org/10.1016/j.gecco.2021.e01548>

879 Liu, J., and Coauthors (2021). Response of global land evapotranspiration to climate change,

880 elevated CO<sub>2</sub>, and land use change. *Agricultural and Forest Meteorology*, 311, 108663.  
 881 <https://doi.org/10.1016/j.agrformet.2021.108663>  
 882 López, P. L., Wanders, N., Schellekens, J., Renzullo, R. J., Sutanudjaja, E. H., Bierkens, M. F. P.  
 883 (2016). Improved large-scale hydrological modelling through the assimilation of streamflow  
 884 and downscaled satellite soil moisture observations. *Hydrology and Earth System Sciences*, 20,  
 885 3059–3076. <https://doi.org/10.5194/hess-20-3059-2016>  
 886 López, P. L., Sutanudjaja, E. H., Schellekens, J., Schellekens, J., Bierkens, M. F. P. (2017).  
 887 Calibration of a large-scale hydrological model using satellite-based soil moisture and  
 888 evapotranspiration products. *Hydrology and Earth System Sciences*, 21, 3125–3144.  
 889 <https://doi.org/10.5194/hess-21-3125-2017>  
 890 Luo, L., Wood, E. F. (2007). Monitoring and predicting the 2007 US drought. *Geophysical Research*  
 891 *Letters*, 34, L22702. <https://doi.org/10.1029/2007GL031673>  
 892 Mann, H. B. (1945). Nonparametric tests against trend. *Econometrica*, 13, 245–259.  
 893 <http://dx.doi.org/10.2307/1907187>  
 894 Martens, B., Miralles, D.G., Lievens, H., van der Schalie, R., de Jeu, R.A.M., Fernández-Prieto, D.,  
 895 Beck, H.E., Dorigo, W.A., Verhoest, N.E.C. (2017). GLEAM v3: satellite-based land  
 896 evaporation and root-zone soil moisture. *Geoscientific Model Development*. 10, 1903–1925.  
 897 <https://doi.org/10.5194/gmd-10-1903-2017>  
 898 Marvel, K., Cook, B. I., Bonfils, C. J. W., Durack, P. J., Smerdon, J. E., Williams, A. P. (2019).  
 899 Twentieth-century hydroclimate changes. *Nature*, 569, 59-65. [https://doi.org/10.1038/s41586-](https://doi.org/10.1038/s41586-019-1149-8)  
 900 019-1149-8  
 901 Massari, C., Brocca, L., Moramarco, T., Trambly, Y., Lescot, J.-F. D. (2014). Potential of soil

moisture observations in flood modelling: estimating initial conditions and correcting rainfall.

*Advance in Water Resources*, 74, 44–53. <https://doi.org/10.1016/j.advwatres.2014.08.004>

McColl, K. A., Alemohammad, S. H., Akbar, R., Konings, A. G., Yueh, S., Entekhabi, D. (2017). The global distribution and dynamics of surface soil moisture. *Nature Geoscience*, 10, 100–104. <https://doi.org/10.1038/ngeo2868>

McKinnon, K.A., Poppick, A. & Simpson, I.R. (2021). Hot extremes have become drier in the United States Southwest. *Nature Climate Change*, 11, 598–604. <https://doi.org/10.1038/s41558-021-01076-9>

Meng, X., Mao, K., Meng F., et al. (2021). A fine-resolution soil moisture dataset for China in 2002–2018. *Earth System Science Data*, 13, 3239–3261. <https://doi.org/10.5194/essd-13-3239-2021>

Min, R., Gu, X., Guan, Y., Zhang, X. (2023). Increasing likelihood of global compound hot-dry extremes from temperature and runoff during the past 120 years. *Journal of Hydrology*, 621, 129553. <https://doi.org/10.1016/j.jhydrol.2023.129553>

Miralles, D. G., Teuling, A. J., Van Heerwaarden, C. C., de Arellano, J. V.-G. (2014). Mega-heatwave temperatures due to combined soil desiccation and atmospheric heat accumulation. *Nature Geoscience*, 7, 345–349. <https://doi.org/10.1038/ngeo2141>

Mo, R. (2003). Efficient algorithms for maximum covariance analysis of datasets with many variables and fewer realizations: A revisit. *Journal of Atmospheric and Oceanic Technology*, 20, 1804–1809. [https://doi.org/10.1175/1520-0426\(2003\)020<1804:EAFMCA>2.0.CO;2](https://doi.org/10.1175/1520-0426(2003)020<1804:EAFMCA>2.0.CO;2)

Ochsner, T. E., Cosh, M. H., Cuenca, R. H., Dorigo, W. A., Draper, C. S., Hagimoto, Y., Kerr, Y. H., Njoku, E. G., Smali, E. E., Zreda, M. (2013). State of the art in large-scale soil moisture monitoring. *Soil Science Society of America Journal*, 77, 1888–1919.



924 <https://doi.org/10.2136/sssaj2013.03.0093>

925 Orlowsky, B., Seneviratne, S. I. (2013). Elusive drought: uncertainty in observed trends and short-

926 and long-term CMIP5 projections, *Hydrology and Earth System Sciences*, 17, 1765–1781.

927 <https://doi.org/10.5194/hess-17-1765-2013>

928 Orth, R., Seneviratne, S. I. (2013). Propagation of soil moisture memory to streamflow and

929 evapotranspiration in Europe. *Hydrology and Earth System Sciences*, 17, 3895–3911.

930 <https://doi.org/10.5194/hess-17-3895-2013>

931 Orth, R., Koster, R. D., Seneviratne, S. I. (2013). Inferring soil moisture memory from streamflow

932 observations using a simple water balance model. *Journal of Hydrometeorology*, 14, 1773–

933 1790. <https://doi.org/10.1175/JHM-D-12-099.1>

934 Orth, R., Zscheischler, J., Seneviratne, S. I. (2016). Record dry summer in 2015 challenges

935 precipitation projections in Central Europe. *Scientific Reports*, 6, 28334.

936 <https://doi.org/10.1038/srep28334>

937 Orth, R., Seneviratne, S. I. (2017). Variability of soil moisture and sea surface temperatures similarly

938 important for warm-season land climate in the Community Earth System Model. *Journal of*

939 *Climate*, 30, 2141–2162. <https://doi.org/10.1175/JCLI-D-15-0567.1>

940 Parinussa, R. M., Lakshmi, V., Johnson, F. M., Sharma, A. (2016). A new framework for monitoring

941 flood inundation using readily available satellite data. *Geophysical Research Letters*, 43, 2599–

942 2605. <https://doi.org/10.1002/2016GL068192>

943 Park, H., Jeong, S., 2021. Leaf area index in Earth system models: how the key variable of

944 vegetation seasonality works in climate projections. *Environmental Research Letters*, 16,

945 034027. <https://doi.org/10.1088/1748-9326/abe2cf>

946 Qin, J., Liang, S., Yang, K., Kaihotsu, I., Liu, R., Koike, T. (2009). Simultaneous estimation of both  
 947 soil moisture and model parameters using particle filtering method through the assimilation of  
 948 microwave signal. *Journal of Geophysical Research: Atmospheres*, 114, D15103.  
 949 <https://doi.org/10.1029/2008JD011358>

950 Qiu, X., Gao, Q., Wang, S., Su, Z. (2016). Comparison of temporal trends from multiple soil  
 951 moisture data sets and precipitation: The implication of irrigation on regional soil moisture  
 952 trend. *International Journal of Applied Earth Observation and Geoinformation*, 48, 17-27.  
 953 <http://dx.doi.org/10.1016/j.jag.2015.11.012>

954 Rasmijn, L. M., van der Schrier, G., Bintanja, R., Barkmeijer, J., Sterl, A., Hazeleger, W. (2018).  
 955 Future equivalent of 2010 Russian heatwave intensified by weakening soil moisture constraints.  
 956 *Nature Climate Change*, 8, 381-385. <https://doi.org/10.1038/s41558-018-0114-0>

957 Rienecker, M. M., et al. (2011). MERRA: NASA's modern-era retrospective analysis for research  
 958 and applications. *Journal of Climate*, 24, 3624–3648. [https://doi.org/10.1175/JCLI-D-11-](https://doi.org/10.1175/JCLI-D-11-00015.1)  
 959 00015.1

960 Rodell, M., et al. (2004). The Global Land Data Assimilation System. *Bulletin of the American*  
 961 *Meteorological Society*, 85, 381–394. <https://doi.org/10.1175/BAMS-85-3-381>

962 Rosenzweig, C., Tubiello, F. N., Goldberg, R., Mills, E., Bloomfield, J. (2002). Increased crop  
 963 damage in the US from excess precipitation under climate change. *Global Environmental*  
 964 *Change*, 12, 197–202. [https://doi.org/10.1016/S0959-3780\(02\)00008-0](https://doi.org/10.1016/S0959-3780(02)00008-0)

965 Rötzer, K., Montzka, C., Vereecken, H. (2015). Spatio-temporal variability of global soil moisture  
 966 products. *Journal of Hydrology*, 522, 187–202. <https://doi.org/10.1016/j.jhydrol.2014.12.038>

967 Rui, H., Beaudoin, H. (2016). README Document for Global Land Data Assimilation System

Version 2 (GLDAS-2) Products.

Ruosteenoja, K., Markkanen, T., Venäläinen, A., Räisänen, P., Peltola, H. (2018). Seasonal soil moisture and drought occurrence in Europe in CMIP5 projections for the 21st century. *Climate Dynamics*, 50, 1177–1192. <https://doi.org/10.1007/s00382-017-3671-4>

Seneviratne, S. I., Corti, T., Davin, E. L., Hirschi, M., Jaeger, E. B., Lehner, I., Orlowsky, B., Teuling, A. J. (2010). Investigating soil moisture–climate interactions in a changing climate: a review. *Earth-Science Reviews*, 99, 125–161. <https://doi.org/10.1016/j.earscirev.2010.02.004>

Shi, W., Tao, F., Liu, J. (2014). Regional temperature change over the Huang-Huai-Hai Plain: the roles of irrigation versus urbanization. *International Journal of Climatology*, 34(4), 1181–1195. <https://doi.org/10.1002/joc.3755>

Siebert, S., Döll, P., Hoogeveen, J., Faures, J., Frenken, K., Feick, S. (2005). Development and validation of the global map of irrigation areas. *Hydrology and Earth System Sciences*, 9(5), 535–547. <https://doi.org/10.5194/hess-9-535-2005>

Slater, L. J., Villarini, G. (2016). Recent trends in U.S. flood risk. *Geophysical Research Letters*, 43(24), 428–436. <https://doi.org/10.1002/2016GL071199>

Su, C.-H., Ryu, D., Dorigo, W., Zwieback, S., Gruber, A., Albergel, C., Reichle, R. H., Wagner, W. (2016). Homogeneity of a global multisatellite soil moisture climate data record. *Geophysical Research Letters*, 43, 11245–11252. <https://doi.org/10.1002/2016GL070458>

Su, F., Duan, X., Chen, D., Hao, Z., Cuo, L. (2013). Evaluation of the global climate models in the CMIP5 over the Tibetan Plateau. *Journal of Climate*, 26, 3187–3208. <https://doi.org/10.1175/JCLI-D-12-00321.1>

Sun, Y., Zhang, X., Ren, G., Zwiers, F. W., Hu, T. (2016). Contribution of urbanization to warming

990 in China. *Nature Climate Change*, 6, 706-710. <https://doi.org/10.1038/NCLIMATE2956>

991 Syed, T., Famiglietti, J., Rodell, M., Chen, J., Wilson, C. (2008). Analysis of terrestrial water storage

992 changes from GRACE and GLDAS. *Water Resources Research*, 44, W02433.

993 <https://doi.org/10.1029/2006WR005779>

994 Van Der Linden, E.C., Haarsma, R.J., Van Der Schrier, G. (2019). Impact of climate model

995 resolution on soil moisture projections in central-western Europe. *Hydrology and Earth System*

996 *Sciences*, 23, 191–206. <https://doi.org/10.5194/hess-23-191-2019>

997 Wang, Y., Mao, J., Hoffman, F.M., Bonfils, C.J.W., Douville, H., Jin, M., Thornton, P.E., Ricciuto,

998 D.M., Shi, X., Chen, H., Wulschleger, S.D., Piao, S., Dai, Y. (2022). Quantification of human

999 contribution to soil moisture-based terrestrial aridity. *Nature Communications*, 13, 6848.

1000 <https://doi.org/10.1038/s41467-022-34071-5>

1001 Yang, Y., Zhang, J., Bao, Z., Ao, T., Wang, G., Wu, H., Wang, J. (2021). Evaluation of Multi-Source

1002 Soil Moisture Datasets over Central and Eastern Agricultural Area of China Using In Situ

1003 Monitoring Network. *Remote Sensing*, 13, 1175. <https://doi.org/10.3390/rs13061175>

1004 Yuan, S., Quiring, S. M., & Leason, Z. T. (2021). Historical changes in surface soil moisture over

1005 the contiguous United States: An assessment of CMIP6. *Geophysical Research Letters*, 48,

1006 e2020GL089991. <https://doi.org/10.1029/2020GL089991>

1007 Taylor, K. E., Stouffer, R. J., Meehl, G. A. (2012). An overview of CMIP5 and the experiment design.

1008 *Bulletin of the American Meteorological Society*, 93, 485–498. [https://doi.org/10.1175/BAMS-](https://doi.org/10.1175/BAMS-D-11-00094.1)

1009 [D-11-00094.1](https://doi.org/10.1175/BAMS-D-11-00094.1)

1010 Teuling, A. J. (2018). A hot future for European droughts. *Nature Climate Change*, 8, 364-365.

1011 <https://doi.org/10.1038/s41558-018-0154-5>

1012 Trenberth, K. E., Dai, A., van der Schrier, G., Jones, P. D., Barichvich, J., Briffa, K. R., Sheffield, J.  
 1013 (2014). Global warming and changes in drought. *Nature Climate Change*, 4, 17-22.

1014 Yin, J., Louise, S., Gu, L., Liao, Z., Guo, S., Gentine, P. (2022). Global increases in lethal compound  
 1015 heat stress: Hydrological drought hazards under climate change. *Geophysical Research Letters*,  
 1016 49, e2022GL100880. <https://doi.org/10.1029/2022GL100880>

1017 Yin, J., Gentine, P., Slater, L., and Co-authors (2023). Future socio-ecosystem productivity  
 1018 threatened by compound drought-heatwave events. *Nature Sustainability*, 6, 259-272.  
 1019 <https://doi.org/10.1038/s41893-022-01024-1>

1020 Yuan, S., Quiring, S. M. (2017). Evaluation of soil moisture in CMIP5 simulations over the  
 1021 contiguous United States using in situ and satellite observations. *Hydrology and Earth System  
 1022 Sciences*, 21, 2203-2218. <https://doi.org/10.5194/hess-21-2203-2017>

1023 Zhang, J., Wang, W. C., Wei, J. (2008). Assessing land-atmosphere coupling using soil moisture  
 1024 from the Global Land Data Assimilation System and observational precipitation. *Journal of  
 1025 Geophysical Research: Atmospheres*, 113, D17119. <https://doi.org/10.1029/2008JD009807>

1026 Zhang, Q., Gu, X., Singh, V. P., Xiao, M., Xu, C.-Y. (2014). Stationarity of annual flood peaks during  
 1027 1951-2010 in the Pearl River basin, China. *Journal of Hydrology*, 519, 3263-3274.  
 1028 <https://doi.org/10.1016/j.jhydrol.2014.10.028>

1029 Zhang, Q., Li, J., Gu, X., Shi, P. (2018). Is the Pearl River basin, China, drying or wetting? Seasonal  
 1030 variations, causes and implications. *Global and Planetary Change*, 166, 48-61.  
 1031 <https://doi.org/10.1016/j.gloplacha.2018.04.005>

1032 Zhuo, L., Han, D., Dai, Q., Islam, T., Srivastava, P. K. S. (2015). Appraisal of NLDAS-2 multi-  
 1033 model simulated soil moistures for hydrological modelling. *Water Resources Management*, 29,

1034 3503-3517. <https://doi.org/10.1007/s11269-015-1011-1>